haematologica
Journal of the Ferrata Storti Foundation

The genetic landscape of extramedullary plasmacytoma: a comparative analysis with extramedullary disease of multiple myeloma

by Antonio Vogelsberg, Julia Salmerón-Villalobos, Anna-Lisa Wilhelmi, Franziska Otto, Aylin Schneider, Barbara Mankel, Eyyub Bag, Ariadna Colmenero, Matthias S Dettmer, Marina Narbaitz, Alexandar Tzankov, Itziar Salaverria, Irina Bonzheim and Falko Fend

Received: November 10, 2025.
Accepted: March 27, 2026.

Citation: Antonio Vogelsberg, Julia Salmerón-Villalobos, Anna-Lisa Wilhelmi, Franziska Otto, Aylin Schneider, Barbara Mankel, Eyyub Bag, Ariadna Colmenero, Matthias S Dettmer, Marina Narbaitz, Alexandar Tzankov, Itziar Salaverria, Irina Bonzheim and Falko Fend. The genetic landscape of extramedullary plasmacytoma: a comparative analysis with extramedullary disease of multiple myeloma.
Haematologica. 2026 Apr 9. doi: 10.3324/haematol.2025.300201 [Epub ahead of print]

The genetic landscape of extramedullary plasmacytoma: a comparative analysis with extramedullary disease of multiple myeloma

Antonio Vogelsberg[1], Julia Salmerón-Villalobos[2], Anna-Lisa Wilhelmi[1], Franziska Otto[1], Aylin Schneider[1], Barbara Mankel[1], Eyyub Bag[1], Ariadna Colmenero[2,3], Matthias S Dettmer[4,5], Marina Narbaitz[6], Alexandar Tzankov[7], Itziar Salaverria[2,8], Irina Bonzheim[1], Falko Fend[1]

[1]Institute of Pathology and Neuropathology, University Hospital and Comprehensive Cancer Center Tuebingen, Tuebingen, Germany

[2]Institut d'Investigacions Biomèdiques August Pi i Sunyer, Barcelona, Spain

[3] University of Barcelona (UB), Barcelona, Spain

[4]Klinikum Stuttgart, Institute of Pathology, Stuttgart, Germany

[5]Institute of Tissue medicine and Pathology, University of Bern, Bern, Switzerland

[6]Servicio de Patología, Instituto de Investigaciones Hematológicas "Mariano R. Castex", Academia Nacional de Medicina, Buenos Aires, Argentina

[7]Institute of Medical Genetics and Pathology, University Hospital Basel, Basel, Switzerland

[8]Centro de Investigación Biomédica en Red de Cáncer (CIBERONC), Madrid, Spain

Running head: Genetic landscape of extramedullary plasmacytoma

Correspondence: Falko Fend (email: falko.fend@med.uni-tuebingen.de)

Data sharing statement: Sequencing data are deposited in the European Nucleotide Archive (PRJEB102117). Copy number data are deposited in ArrayExpress (E-MTAB-16327).

Disclosures: The authors have no conflicts of interest to disclose.

Acknowledgements: The authors would like to thank the staff of the immunohistochemistry and molecular diagnostics laboratories for their excellent technical support. AV was supported by the Junior Clinician Scientist Program of the University Hospital Tuebingen (grant number 516-0-0), and A-LW was supported by the IZKF Promotionskolleg of the University Tuebingen (grant number 2022-2-20).

Author Contributions: FF and AV conceived and designed the study, selected and reviewed the cases, supervised the experimental work and data analysis, and wrote the manuscript. A-LW was involved in case selection and performed the NGS experiments. FO, AS, and IB supervised the experimental work and performed NGS data analysis. JS-V and IS performed the CN analysis and helped to write the manuscript. AC performed the ASCAT analyses and contributed to data interpretation. BM performed FISH analysis. EB provided bioinformatic support and performed statistical analyses. AT, MSD, and MN contributed cases and provided clinical information. All authors revised the manuscript.

Abstract

Extramedullary (or extraosseous) plasmacytoma (EMP) is a localized plasma cell neoplasm lacking apparent bone marrow involvement and other features of multiple myeloma (MM). The prognosis is usually favorable and progression to MM is infrequent. The genetic landscape of EMP remains largely unknown. Importantly, EMP must be distinguished from extramedullary disease of MM (EMD), which typically exhibits aggressive behavior. We performed a comprehensive molecular analysis of EMP (n=24) in comparison to EMD (n=24) using fluorescence *in situ* hybridization (FISH), copy number (CN) profiling, and targeted next-generation sequencing. Overall, EMP shared several genetic features with MM, but exhibited markedly lower complexity than EMD. EMP revealed a mean of 4.3 CN changes vs. 19.3 in EMD ($p<0.001$). IGH breaks were detected in 6 EMP and 10 EMD, and hyperdiploidy in 10 and 14 cases, respectively. Gains of 1q21 occurred in 9 EMP and 15 EMD ($p=0.045$). Likewise, EMP harbored fewer mutations (median 2.0 vs. 3.0; $p<0.01$), yet was enriched for *TRAF3* mutations, detected in 6 cases, which were absent in EMD ($p=0.022$). In contrast, EMD more frequently harbored mutations associated with advanced MM, including *NRAS/KRAS* ($p<0.01$), *TP53*, *TENT5C*, *ARID1A*, and *ATM*. In conclusion, we demonstrate that EMP shows a significantly less complex and, in part, distinct genetic profile compared to EMD. This may aid in differentiating the two entities in diagnostically challenging cases and could help to identify EMP with an increased risk of progression.

Introduction

Multiple myeloma (MM) is a systemic plasma cell neoplasm defined by bone marrow (BM) infiltration in combination with myeloma-associated organ damage and/or specific myeloma-defining biomarkers (summarized by the SLiM-CRAB criteria).[1] MM follows a variable clinical course, but characteristically evolves in a stepwise manner, starting from its indolent precursor monoclonal gammopathy of undetermined significance (MGUS) and ultimately leading to biologically advanced manifestations such as extramedullary disease (EMD), which frequently occurs in relapsed disease, typically exhibits aggressive behavior, and carries a poor prognosis.[2-4] The genetic events initiating this process are either (1) trisomies of three or more of the odd-numbered chromosomes 3, 5, 7, 9, 11, 15, 19, 21, a constellation known as hyperdiploidy (HD), or (2) rearrangements of the immunoglobulin heavy chain (IGH) locus involving *NSD2* or members of the *CCND* and *MAF* gene families.[5] Secondary events driving disease progression are heterogeneous and include loss of 13q14, aberrations of chromosome 1, alterations of *MYC* and *TP53*, as well as mutations affecting the NF-κB and MAPK/ERK pathways.[6,7] Several alterations, among them gains of *CKS1B* (1q21.3–q22) and deletions of *CDKN2C* (1p32.3) and *TP53* (17p13.1), have been associated with an unfavorable prognosis and are enriched in patients with EMD.[3,8,9]

Importantly, EMD must be distinguished from solitary extramedullary (or extraosseous) plasmacytoma (EMP). EMP is a localized plasma cell neoplasm that most commonly arises in the upper aerodigestive tract and lacks overt BM infiltration and other defining features of MM.[5,10,11] In contrast to EMD, EMP generally shows a favorable prognosis and can be effectively managed with local therapy.[11,12] Still, a subset of patients (10–30%) progresses to MM, and although some adverse features have been proposed, such as sinonasal localization and minimal BM involvement detected by flow cytometry, predicting an unfavorable course continues to be a subject of research.[12-14] Previous studies have shown that EMP – while morphologically and immunophenotypically often indistinguishable from EMD – tends to display more mature cytology, lower proliferative activity, and less frequent aberrant expression of CD56 and Cyclin D1.[15-18] Genetically, EMP appears to harbor HD and recurrent IGH translocations at a frequency comparable to MM, with the exception of *CCND1* rearrangements, which seem to be virtually absent.[15,17,18] The mutational profile and the prevalence of secondary alterations, including those deemed high-risk in MM, however, remain largely unknown.[15]

Here, we conducted the first comprehensive molecular analysis of EMP in comparison with EMD, focusing on secondary alterations and employing fluorescence *in situ* hybridization (FISH), copy-number (CN) profiling, and targeted next-generation sequencing (NGS),

complemented by immunohistochemical analyses, to elucidate the biological basis of the distinct behavior of EMP and possibly take a first step toward its molecular risk stratification.

Methods

Sample selection

Cases were identified by searching the archives of the Institute of Pathology of Tuebingen University Hospital, Germany, and the Institute of Medical Genetics and Pathology of Basel University Hospital, Switzerland, for formalin-fixed and paraffin-embedded (FFPE) tissue samples from patients diagnosed with EMP or EMD. Cases were reviewed by experienced hematopathologists (FF, Tuebingen; AT, Basel) and diagnosed in accordance with the International Consensus Classification of Myeloid and Lymphoid Neoplasms and the 5th edition of the World Health Organization Classification of Haematolymphoid Tumours.[5,10] In one EMD case, multiple samples were analyzed (supplemental material). The study was approved by the Ethics Committee of the University of Tuebingen (approval number 462/2022BO2).

Immunohistochemistry (IHC) and FISH

Samples were stained for MUM1, CD138, Cyclin D1, immunoglobulin (IG) kappa and lambda light chains, MIB-1, p53, MYC, and EBV-encoded RNA (in EMP cases only), and analyzed by FISH for IGH (14q32.33) rearrangements, gains of *CKS1B* (1q21.3–q22), losses of *CDKN2C* (1p32.3) and *TP53* (17p13.1), as well as gains of 5p15.2–p15.3, 9q22.3–q31, and 15q22.3 as a surrogate for HD. For additional information, including further characterization of IGH translocations in EMP, see the supplemental material.

DNA extraction and CN analysis

DNA was extracted from paraffin sections using the Maxwell RSC Instrument (Promega, Mannheim, Germany). Samples with sufficient material (15 EMP and 10 EMD) were hybridized on the OncoScan FFPE Array platform (Thermo Fisher Scientific, Waltham, MA, USA). CN alterations (CNA), i.e., gains and losses, as well as CN neutral loss of heterozygosity (CNN-LOH) regions, were assessed and inspected using Nexus Copy Number software (version 9.0; BioDiscovery, Hawthorne, CA, USA). Further details, particularly regarding integration with FISH results, are provided in the supplemental material.

Targeted NGS

Targeted NGS was performed on the Ion GeneStudio S5 Prime System (Thermo Fisher Scientific), employing two Ion AmpliSeq custom panels (Thermo Fisher Scientific) covering 89

genes frequently altered in MM and B-cell lymphoma (Supplemental Tables S1 and S2). Library preparation, sequencing, and data analysis are described in the supplemental material.

Statistical analysis

Statistical analyses were performed using R (version 4.4.3; R Foundation for Statistical Computing, Vienna, Austria). Comparisons were conducted using non-parametric tests (Mann-Whitney U and Fisher's exact test), and correlations were assessed using Spearman correlation. All tests were two-sided, with $p < 0.05$ considered significant. Most genetic comparisons were exploratory and not adjusted for multiple testing, and p-values should be interpreted accordingly. The comparison regarding enrichment of CN regions was performed using Fisher's exact test, considering a minimum of five altered cases for adjusted p-value calculation.

Results

Patient characteristics and clinical features

Forty-eight cases were included, comprising 24 EMP and 24 EMD. Among the EMP cases, the median age at diagnosis was 63 years (range 18–93), with a male predominance (M:F = 3:1), and the upper aerodigestive tract being the most common site of manifestation (Table 1; Supplemental Figure S1). None of the EMP patients showed evidence of MM based on clinical assessment, imaging, and a trephine BM biopsy (available in 21/24 cases). In addition, no clonal plasma cells were detected by flow cytometry in the BM of any of the 13 patients with available data, and only 4/21 patients with available data showed a low-level paraprotein. Most patients were treated with surgery combined with radiotherapy or radiotherapy alone and achieved complete remission. Five patients experienced a locoregional relapse, with follow-up times ranging between 3 and 194 months. Only one patient (case 11) showed progression to MM and died from the disease. In the EMD group, the median age at disease onset was 66 years (range 47–86) with a more balanced gender distribution (M:F = 1.18:1). EMD most commonly involved soft tissues at various sites, with 11/24 cases developing in patients with previously diagnosed MM, while in the remaining cases, EMD represented the first manifestation of systemic disease. Only 2/16 EMD patients with available data achieved complete remission (Supplemental Table S3; Supplemental Figure S2).

Morphology and immunophenotype

The EMP displayed typical morphology, characterized by monotonous sheets of plasma cells with variable degrees of atypia, but predominantly mature cytology (Figure 1). Immature cytology, defined by prominent nucleoli, an increased nucleus-to-cytoplasm ratio, open/blastoid nuclear chromatin and/or anaplasia, was observed in only 2/24 EMP compared

to 6/24 EMD. Of note, one of the EMP with immature cytology (case 16) was the only EBV-positive sample in our cohort (Table 2). By immunohistochemistry, EMP demonstrated significantly lower proliferation rates (EMP vs. EMD: median 19.8% vs. 42.2%; $p < 0.001$), lower MYC expression ($p = 0.001$), as well as less frequent CD56 expression (8/24 vs. 16/24; $p = 0.043$). Likewise, Cyclin D1 positivity was rare in EMP compared to EMD (2/24 vs. 9/24; $p = 0.039$). Notably, one EMP (case 23) showed strong and homogeneous expression of Cyclin D1, typically only observed in MM with a rearrangement of *CCND1*, which was confirmed by FISH. This was also the only EMP demonstrating aberrant, albeit focal, strong p53 staining (compared to 4/22 EMD showing aberrant staining) and the only EMP initially treated with chemotherapy due to an unusual presentation with involvement of the lung and mediastinal lymph nodes, despite never showing BM infiltration. No clear trend toward higher proliferation or other features was observed in cases that experienced a relapse.

FISH and CN profile

An IGH break, indicative of a translocation involving the IGH locus, was detected by FISH in 6/24 EMP and 10/22 EMD. Apart from case 23, no EMP showed an IGH translocation involving any of the tested partner loci (*CCND1*, *NSD2*, *MAF*, *MAFB*). By combining FISH and CN analyses, HD was demonstrated in 10/24 EMP and 14/20 EMD. Regarding secondary alterations, losses of *CDKN2C* (1p32.3) were detected at similar frequencies in EMP (3/24) and EMD (4/22), although homozygous deletions were exclusively observed in EMD (2/22). In contrast, gains of *CKS1B* (1q21.3–q22) were less frequent in EMP than in EMD (9/24 vs. 15/22; $p = 0.045$), with amplifications (>3 copies by FISH) detected in 4/24 EMP and 7/22 EMD, respectively. In 6/9 EMP compared to only 4/15 EMD, the *CKS1B* gain occurred concomitantly with a gain of *CDKN2C*, most likely reflecting trisomy 1. Losses of *TP53* (17p13.1) were also less frequent in EMP (5/24) than in EMD (8/22). In two EMP and one EMD, del(17p) occurred in the context of a chromosome 17 gain, resulting in a relative 17p loss with retention of two *TP53* copies.

Based exclusively on OncoScan-derived CN data, available for 15 EMP and 10 EMD, EMP exhibited significantly lower genomic complexity, with a mean of 4.3 CNA (range 0–14) and 0.5 CNN-LOH events per case, in contrast to 19.3 CNA (range 7–43) and 3.0 CNN-LOH events per case in EMD (both $p < 0.001$; Figure 2). Notably, the highest genomic complexity among EMP samples, including a polyploid genome, was observed in case 11, which progressed to MM, whereas no clear trend toward increased CNA burden or specific alterations was seen in cases that experienced a local EMP relapse (Supplemental Tables S4-S5). The most frequent CNA in EMP were gains of 9q21.11–q34.3 and losses of 8p23.3–p21.2 (each in 4/15 samples), followed by deletions of 1p33–p13.2 (harboring *CDKN2C*) and gains of 1q21.1–q44 (involving *CKS1B*; each in 3/15 samples). In comparison, loss of 13q14.11–q31.2 (including *RB1* and

DIS3), as well as gains of 5p, 15q11.1–q21.3, 19p, 6p, and 3q23–q26.1, were significantly enriched in EMD.

A comparison of EMP with CN data from two previously published MM cohorts revealed significantly lower complexity in EMP (mean 4.3 CNA vs 12.9; $p < 0.001$) as well as a trend toward fewer CNN-LOH events (mean 0.5 vs. 1.3; $p = 0.2$; Supplemental Figure S5).[6,19] MM samples were comparatively enriched for gains at 1q21.1–q22, 7q31.1–q32.1, 11q, and entire chromosomes 3, 5, 9, 15, 19, and 21. Further details are available in the supplemental material.

Mutational analysis

Targeted NGS of EMP revealed a significant variability in the number of mutations per case (median 2.0 mutations; mean 2.41; range 0–12) and a broad distribution of affected genes. *TRAF3* was the most commonly mutated gene in EMP, affected in 6/24 (25%) samples. Notably, in three samples (cases 3, 11, and 24), the variant allele frequency (VAF) exceeded 50%, with another sample (case 19) showing three distinct *TRAF3* mutations – findings indicative of a biallelic or hemizygous event (Figure 3). Accordingly, a heterozygous loss and LOH of the chromosomal 14q32.32 region, which encompasses *TRAF3*, were identified in the CNA analysis of cases 3 and 11, respectively (Supplemental Table S4). Other genes recurrently mutated in EMP included *BRAF* (4/24 EMP, all p.V600E), *HIST1H1E* (3/24), as well as *NRAS*, *KMT2D*, *PCLO*, *PLCG2*, *POT1*, *NFKBIA*, and *PIM1* (each in 2/24 samples). The number of mutations was positively correlated with the CNA burden (Spearman $\rho = 0.54$, $p = 0.04$). Accordingly, case 11, which progressed to MM, demonstrated above-average complexity (7 mutations). The number of mutations was also positively correlated with the proliferation rate in EMP (Spearman $\rho = 0.42$, $p = 0.04$). No consistent association between relapse and mutational complexity was observed.

EMD showed a higher number of mutations per case (median 3.0; mean 3.63; range 1–8) compared to EMP ($p = 0.008$). In EMD, the most frequently mutated gene was *NRAS* (11/24 samples), followed by *PCLO* (6/24), *KRAS* and *TP53* (each in 5/24), *KMT2D*, *ATM*, *ARID1A*, and *TENT5C* (each in 4/24), as well as *BRAF* and *ROBO2* (each in 3/24). Of note, there was a trend toward higher mutational complexity in EMD arising as a late event in patients with previously diagnosed MM (mean 4.18 mutations; range 1–8), compared to EMD representing the primary manifestation (mean 3.15; range 1–5), with the latter being on average still more complex than EMP.

In comparison with EMP, EMD samples were significantly enriched for *RAS* alterations (3/24 vs. 16/24; $p < 0.001$), with *NRAS* mutations detected in 2/24 EMP and 11/24 EMD samples ($p < 0.01$), and *KRAS* mutated in 1/24 EMP and 5/24 EMD. In contrast, *BRAF* mutations occurred at a similar frequency in both groups (4/24 EMP vs. 3/24 EMD). *TP53* was also more

frequently mutated in EMD (5/24) than in EMP (1/24). Notably, in all *TP53*-mutated cases with available FISH data (i.e., all except case 25), a concurrent del(17p) was detected, consistent with biallelic inactivation. In line with this, all mutated EMD samples, including case 25, demonstrated a *TP53* VAF exceeding 50% and exhibited an aberrant p53 staining pattern. In contrast, the only *TP53*-mutated EMP (case 23) showed a VAF of 22%, suggesting a subclonal event, as supported by the only focal overexpression of p53. Additional genes more frequently altered in EMD included *PCLO* (2/24 EMP vs. 6/24 EMD), *TENT5C* and *ATM* (each 0/24 vs. 4/24), and *ARID1A* (1/24 vs. 4/24), as well as *ROBO2* (0/24 vs. 3/24). In contrast, *TRAF3* mutations were not detected in EMD (6/24 EMP vs. 0/24 EMD; $p = 0.022$), making it the only gene significantly enriched in EMP.

Discussion

This study provides the first comprehensive molecular characterization of EMP, integrating CNA, FISH, and mutational data, in addition to histopathologic and immunophenotypic features. We demonstrate that EMP shares several genetic features with MM, but exhibits significantly lower genomic complexity and a partially distinct mutational profile compared to EMD, which usually occurs in advanced MM. These findings support the concept that most EMP represent early, localized plasma cell neoplasms, provide a genetic basis for their more indolent behavior, and may help to identify EMP cases with an increased risk of progression.

The clinical characteristics of our EMP cohort, including the predilection for the upper respiratory tract and the favorable response to localized therapy with few relapses and only one case progressing to MM, are consistent with the literature and stand in stark contrast to the aggressive behavior observed in EMD.[12,20] Likewise, the less common occurrence of immature morphology, the lower proliferation rate, the less frequent aberrant expression of CD56, and the infrequent overexpression of p53 and Cyclin D1 in EMP are in agreement with published data.[16] In concordance with findings by Billecke *et al.*, MYC expression was also significantly less frequent in EMP.[21] Of note, MGUS is typically negative for MYC as well, and higher MYC expression has been associated with shorter survival in MM.[22] Intriguingly, the two EMP with MYC expression in >30% of cells (cases 14 and 16) were the only ones displaying immature morphology and demonstrated high proliferation, which might suggest more aggressive behavior. However, the relatively short follow-up period in both patients precludes a firm conclusion. In line with previous studies from our group and others, only 2/24 EMP, compared to 9/24 EMD, showed Cyclin D1 expression. Surprisingly, one EMP (case 23) showed strong and homogeneous expression of Cyclin D1 due to an underlying *CCND1* rearrangement – a finding that, to our knowledge, has only been reported once in an EMP patient who subsequently developed MM.[15,23] Our case displayed an unusual clinical course with involvement of the lung and mediastinal lymph nodes, ultimately requiring chemotherapy

and autologous stem cell transplantation. Notably, however, the patient did not fulfill the criteria for MM at any point, despite thorough clinical evaluation. The second Cyclin D1-positive EMP, which progressed to MM, showed only weak and heterogeneous staining, typically associated with additional copies of *CCND1* or HD, which was confirmed by FISH.[18,24,25] Importantly, this staining pattern has previously been associated with aggressive behavior and development of MM in EMP.[18] Therefore, in keeping with previous reports, our data support that expression of Cyclin D1 in a putative EMP should prompt an intensive search for an underlying systemic plasma cell neoplasm and might indicate aggressive behavior.[16]

MM and its precursors can be divided into two genetic groups based on their primary genetic alterations: those with HD and those harboring recurrent IGH translocations.[5] The frequency of HD and IGH translocations in our EMP cohort was comparable to previously published data.[15] In comparison to EMD, there was a larger proportion of EMP samples that lacked both alterations (46% vs. 9%), which is in line with the overall lower genomic complexity and resembles observations made in MGUS.[26] Of note, a subset of IGH translocations in EMD, particularly in cases also harboring HD, may represent secondary events, such as rearrangements involving *MYC*, that arose during disease progression.[3]

The CNA profile of EMP, although less complex overall, was reminiscent of MM: gains of 9q and losses of 8p, the most common CNA next to alterations of chromosome 1, are frequently found in MM and its precursors, with the former most often occurring in the context of trisomy 9.[6,27] Consistent with its more aggressive course, EMD not only carried a higher CNA burden but was also enriched for alterations that are significantly more frequent in MM than in MGUS, such as gains of 19p and 6p, suggesting that these events occur during disease progression.[6] Surprisingly, del(13q) was also enriched in EMD and detected in only 2/15 EMP (13%), which contrasts with previous studies reporting deletions of 13q in up to 40% of cases.[15,17] This discrepancy may, in part, be due to sensitivity differences between array-based methods and FISH.[28] Alternatively, the apparently higher frequency of 13q loss in FISH-based studies may be attributable to nuclear sectioning artifacts.[15]

Two secondary alterations, loss of *CDKN2C* and gain of *CKS1B*, were detected in EMP at frequencies similar to those observed in MM.[29,30] Both alterations have also been observed in MGUS, supporting their potential role as relatively early clonal events in plasma cell neoplasms.[26] Nevertheless, they have more commonly been associated with aggressive behavior and extramedullary spread in MM.[30] This was also reflected in our cohort, given the significant enrichment of 1q gains in the EMD samples, as well as the more frequent occurrence of 1q amplifications in the latter, which has been linked to a particularly poor prognosis.[30] Likewise, biallelic inactivation of *CDKN2C*, also shown to define a subset of ultra-high-risk myeloma, was only found in EMD.[31] Notably, 6/9 EMP with a 1q gain, including three

cases with amplification, showed concurrent gains of 1p, most likely as a result of gains of the entire chromosome. Although chromosome 1 gains are recognized as one mechanism of 1q gain, it remains unclear whether this pattern conveys the same poor prognosis.[32,33] Loss of 17p13.1 (*TP53*), an alteration detected in around 8% of MM and associated with an unfavorable clinical course, was also surprisingly common in EMP, although, again, less frequent than in EMD.[7] Importantly, in two out of five EMP with a del(17p), compared to only one out of eight EMD, the deletion occurred in the context of a chromosome 17 gain, which resulted in a relative 17p loss with two *TP53* copies remaining. Myelomas harboring this constellation show survival comparable to those with a typical del(17p).[34] The clinical implications of these presumed high-risk alterations and higher genomic complexity in EMP remain to be elucidated, as no clear association with more aggressive behavior or relapse was observed in our cohort. Of note, however, the case that progressed to MM exhibited the highest CNA complexity among all EMP.

The mutational analysis of EMP, to our knowledge the first dataset published in adults, revealed several recurrently mutated genes, including *TRAF3*, *BRAF*, *NRAS*, *PCLO*, and *NFKBIA*, which have also been implicated in the pathogenesis of MM.[7,35] Intriguingly, despite the overall lower mutational burden, mutations of *TRAF3* were detected in 25% of EMP and were significantly enriched compared to our EMD cohort. Inactivation of the negative regulator *TRAF3* is a well-recognized mechanism of NF-κB activation in MM, resulting from mutations and/or deletions involving 14q32, which have been reported in approximately 10–15% of cases.[7,36-38] In four of six *TRAF3*-mutated EMP, biallelic inactivation was suspected and confirmed in two cases by the detection of a concurrent deletion and LOH of the 14q32 region, respectively. Biallelic *TRAF3* inactivation has been described in MM, although more commonly in the relapse setting, where it does not appear to confer a poor prognosis.[39] In fact, *TRAF3* mutations have been linked to a favorable outcome in MM, which is consistent with their absence in our EMD cohort and the rarity of such mutations in prior reports addressing EMD.[3,9,30] Notably, *NFKBIA*, which is also involved in the NF-κB pathway, was mutated exclusively in EMP as well.[36]

In turn, EMD was significantly enriched for *RAS* mutations (*NRAS* and *KRAS*), which are part of the MAPK/ERK pathway and among the most commonly mutated genes in MM.[7] In line with our findings, these mutations have been reported to be overrepresented in patients with EMD and associated with poor prognosis in MM, although they have also occasionally been detected at the MGUS stage.[9,26,40,41] Interestingly, *BRAF* mutations, despite their similar association with unfavorable outcome and involvement in the MAPK pathway, were detected at comparable frequencies in both groups, with all mutations in EMP being the canonical p.V600E.[41-43] Several additional genes more commonly mutated in the EMD group have been associated with EMD

and/or poor survival in MM, including *ARID1A*, *ATM*, *TENT5C*, *DIS3*, *ROBO2*, and, in particular, *TP53.*[9,30,42,44] Of note, all *TP53*-mutated EMD demonstrated a concurrent del(17p), consistent with biallelic inactivation, which is a hallmark of ultra-high-risk MM with a dire prognosis.[30] Surprisingly, this molecular constellation was also observed in one EMP (case 23), which – although the *TP53* mutation was only subclonal – likely contributed to its unusual clinical course. Nevertheless, future studies on EMP are needed to clarify the prognostic impact of individual mutations and their overall number, the latter being associated with increased proliferative activity and CNA burden but not generally higher in relapsing cases. Interestingly, in contrast to our study, a recent investigation of a small pediatric EMP cohort did not identify MM-type alterations, pointing to potential biological differences in this rare EMP subtype.[45] Of note, case 1, the only sample lacking detectable aberrations in our series, likewise arose in an 18-year-old male.

Importantly, EMP occasionally needs to be separated from entities other than EMD. Case 16, characterized by EBV positivity, immature cytology, MYC expression, and high proliferation, needed to be distinguished from plasmablastic lymphoma (PBL). However, as EBV-positive EMP is well described and frequently exhibits features similar to our case, and given that none of the recently proposed criteria for PBL by Zhou *et al.* were met, a diagnosis of EMP was rendered.[46,47] Intriguingly, case 14, notably the second EMP with immature cytology and high MYC expression, harbored an unusual and complex mutational profile, including mutations of *TCF3* and *ID3*, which are commonly detected in Burkitt lymphoma.[48] Despite this, the case demonstrated clear-cut morphologic and immunophenotypic features of EMP and lacked a *MYC* translocation.

Established prognostic parameters are sparse in EMP and so far, no genetic risk factors have been defined. However, it is tempting to speculate that, in line with recent data for solitary plasmacytoma of bone, high-risk genetics might indicate an increased risk of and shorter time to progression in EMP as well.[49] Of note, both cases (11 and 23) that showed progression or more extensive disease had genetic features associated with higher risk in MM. Ultimately, the genetic profile might enable a separation into progressive and stable forms of local plasma cell neoplasms.

Given the modest cohort size and the reliance on archival FFPE tissue, which likely reduced sensitivity for detecting subclonal alterations in a subset of samples, our findings warrant confirmation in larger cohorts. These future studies should also more extensively characterize IGH translocations in EMP, as the translocation partner was only identified in a single case. Even so, this study provides the first comprehensive analysis of genetic alterations in EMP and offers novel insights into its biology, further highlighting the differences from EMD.

References

1. Rajkumar SV, Dimopoulos MA, Palumbo A, et al. International Myeloma Working Group updated criteria for the diagnosis of multiple myeloma. Lancet Oncol. 2014;15(12):e538-e548.
2. Schavgoulidze A, Cazaubiel T, Perrot A, Avet-Loiseau H, Corre J. Multiple myeloma: heterogeneous in every way. Cancers (Basel). 2021;13(6):1285.
3. Bhutani M, Foureau DM, Atrash S, Voorhees PM, Usmani SZ. Extramedullary multiple myeloma. Leukemia. 2020;34(1):1-20.
4. Avivi I, Cohen YC, Suska A, et al. Hematogenous extramedullary relapse in multiple myeloma - a multicenter retrospective study in 127 patients. Am J Hematol. 2019;94(10):1132-1140.
5. Campo E, Jaffe ES, Cook JR, et al. The international consensus classification of mature lymphoid neoplasms: a report from the Clinical Advisory Committee. Blood. 2022;140(11):1229-1253.
6. López-Corral L, Sarasquete ME, Beà S, et al. SNP-based mapping arrays reveal high genomic complexity in monoclonal gammopathies, from MGUS to myeloma status. Leukemia. 2012;26(12):2521-2529.
7. Walker BA, Mavrommatis K, Wardell CP, et al. Identification of novel mutational drivers reveals oncogene dependencies in multiple myeloma. Blood. 2018;132(6):587-597.
8. Gagelmann N, Eikema DJ, Koster L, et al. Tandem autologous stem cell transplantation improves outcomes in newly diagnosed multiple myeloma with extramedullary disease and high-risk cytogenetics: a study from the Chronic Malignancies Working Party of the European Society for Blood and Marrow Transplantation. Biol Blood Marrow Transplant. 2019;25(11):2134-2142.
9. Zanwar S, Novak J, Gonsalves W, et al. Extramedullary myeloma is genomically complex and characterized by near-universal MAPK pathway alterations. Blood Adv. 2025;9(15):3979-3987.
10. Cree IA. The WHO Classification of Haematolymphoid Tumours. Leukemia. 2022;36(7):1701-1702.
11. Caers J, Paiva B, Zamagni E, et al. Diagnosis, treatment, and response assessment in solitary plasmacytoma: updated recommendations from a European Expert Panel. J Hematol Oncol. 2018;11(1):10.
12. Venkatesulu B, Mallick S, Giridhar P, Upadhyay AD, Rath GK. Pattern of care and impact of prognostic factors on the outcome of head and neck extramedullary plasmacytoma: a systematic review and individual patient data analysis of 315 cases. Eur Arch Otorhinolaryngol. 2018;275(2):595-606.
13. Paiva B, Chandia M, Vidriales MB, et al. Multiparameter flow cytometry for staging of solitary bone plasmacytoma: new criteria for risk of progression to myeloma. Blood. 2014;124(8):1300-1303.
14. Charalampous C, Claveau JS, Kapoor P, et al. Solitary Plasmacytoma: Single institution experience and systematic review and meta-analysis of clinical outcomes. Blood Adv. 2025;9(7):1559-1570.
15. Bink K, Haralambieva E, Kremer M, et al. Primary extramedullary plasmacytoma: similarities with and differences from multiple myeloma revealed by interphase cytogenetics. Haematologica. 2008;93(4):623-626.
16. Kremer M, Ott G, Nathrath M, et al. Primary extramedullary plasmacytoma and multiple myeloma: phenotypic differences revealed by immunohistochemical analysis. J Pathol. 2005;205(1):92-101.
17. Boll M, Parkins E, O'Connor SJ, Rawstron AC, Owen RG. Extramedullary plasmacytoma are characterized by a 'myeloma-like' immunophenotype and genotype and occult bone marrow involvement. Br J Haematol. 2010;151(5):525-527.
18. Kojima M, Motoori T, Tamaki Y, et al. Cyclin D1 protein overexpression in extramedullary plasmacytoma: a clinicopathologic study of 11 cases. J Clin Exp Hematop. 2009;49(1):53-56.

19. Paiva B, Corchete LA, Vidriales MB, et al. Phenotypic and genomic analysis of multiple myeloma minimal residual disease tumor cells: a new model to understand chemoresistance. Blood. 2016;127(15):1896-1906.
20. de Waal EG, Leene M, Veeger N, et al. Progression of a solitary plasmacytoma to multiple myeloma. A population-based registry of the northern Netherlands. Br J Haematol. 2016;175(4):661-667.
21. Billecke L, Murga Penas EM, May AM, et al. Cytogenetics of extramedullary manifestations in multiple myeloma. Br J Haematol. 2013;161(1):87-94.
22. Chng WJ, Huang GF, Chung TH, et al. Clinical and biological implications of MYC activation: a common difference between MGUS and newly diagnosed multiple myeloma. Leukemia. 2011;25(6):1026-1035.
23. Parkins E, Boll M, O'Connor SJ, Rawstron AC, Owen RG. Extramedullary plasmacytoma with a t(11;14)(q13;q32) and aggressive clinical course. Leuk Lymphoma. 2010;51(7):1360-1362.
24. Bergsagel PL, Chesi M. V. Molecular classification and risk stratification of myeloma. Hematol Oncol. 2013;31 Suppl 1(0 1):38-41.
25. Specht K, Haralambieva E, Bink K, et al. Different mechanisms of cyclin D1 overexpression in multiple myeloma revealed by fluorescence in situ hybridization and quantitative analysis of mRNA levels. Blood. 2004;104(4):1120-1126.
26. Mikulasova A, Wardell CP, Murison A, et al. The spectrum of somatic mutations in monoclonal gammopathy of undetermined significance indicates a less complex genomic landscape than that in multiple myeloma. Haematologica. 2017;102(9):1617-1625.
27. Walker BA, Leone PE, Chiecchio L, et al. A compendium of myeloma-associated chromosomal copy number abnormalities and their prognostic value. Blood. 2010;116(15):e56-65.
28. Leeksma AC, Baliakas P, Moysiadis T, et al. Genomic arrays identify high-risk chronic lymphocytic leukemia with genomic complexity: a multi-center study. Haematologica. 2021;106(1):87-97.
29. Boyle EM, Blaney P, Stoeckle JH, et al. Multiomic Mapping of Acquired Chromosome 1 Copy-Number and Structural Variants to Identify Therapeutic Vulnerabilities in Multiple Myeloma. Clin Cancer Res. 2023;29(19):3901-3913.
30. Walker BA, Mavrommatis K, Wardell CP, et al. A high-risk, Double-Hit, group of newly diagnosed myeloma identified by genomic analysis. Leukemia. 2019;33(1):159-170.
31. Schavgoulidze A, Talbot A, Perrot A, et al. Biallelic deletion of 1p32 defines ultra-high-risk myeloma, but monoallelic del(1p32) remains a strong prognostic factor. Blood. 2023;141(11):1308-1315.
32. Clarke SE, Fuller KA, Erber WN. Chromosomal defects in multiple myeloma. Blood Rev. 2024;64:101168.
33. Hanamura I. Gain/amplification of chromosome arm 1q21 in multiple myeloma. Cancers (Basel). 2021;13(2):256.
34. Lakshman A, Painuly U, Rajkumar SV, et al. Natural history of multiple myeloma with de novo del(17p). Blood Cancer J. 2019;9(3):32.
35. Rasche L, Chavan SS, Stephens OW, et al. Spatial genomic heterogeneity in multiple myeloma revealed by multi-region sequencing. Nat Commun. 2017;8(1):268.
36. Cardona-Benavides IJ, de Ramón C, Gutiérrez NC. Genetic abnormalities in multiple myeloma: prognostic and therapeutic implications. Cells. 2021;10(2):336.
37. Manier S, Salem KZ, Park J, Landau DA, Getz G, Ghobrial IM. Genomic complexity of multiple myeloma and its clinical implications. Nat Rev Clin Oncol. 2017;14(2):100-113.
38. Keats JJ, Fonseca R, Chesi M, et al. Promiscuous mutations activate the noncanonical NF-kappaB pathway in multiple myeloma. Cancer Cell. 2007;12(2):131-144.
39. Weinhold N, Ashby C, Rasche L, et al. Clonal selection and double-hit events involving tumor suppressor genes underlie relapse in myeloma. Blood. 2016;128(13):1735-1744.
40. Liu Y, Jelloul F, Zhang Y, et al. Genetic basis of extramedullary plasmablastic transformation of multiple myeloma. Am J Surg Pathol. 2020;44(6):838-848.

41. Perroud C, Thurian D, Andres M, et al. Effect of MAPK activation via mutations in NRAS, KRAS and BRAF on clinical outcome in newly diagnosed multiple myeloma. Hematol Oncol. 2023;41(5):912-921.
42. Boyle EM, Ashby C, Tytarenko RG, et al. BRAF and DIS3 Mutations Associate with Adverse Outcome in a Long-term Follow-up of Patients with Multiple Myeloma. Clin Cancer Res. 2020;26(10):2422-2432.
43. Andrulis M, Lehners N, Capper D, et al. Targeting the BRAF V600E mutation in multiple myeloma. Cancer Discov. 2013;3(8):862-869.
44. Walker BA, Boyle EM, Wardell CP, et al. Mutational spectrum, copy number changes, and outcome: results of a sequencing study of patients with newly diagnosed myeloma. J Clin Oncol. 2015;33(33):3911-3920.
45. Oschlies I, Richter J, Alfert A, et al. Extramedullary plasmacytoma in children is a genetically distinct localized neoplasia curable by surgical resection. Blood Adv. 2025;9(15):3909-3918.
46. Zhou T, Cheng J, Karrs J, et al. Clinicopathologic and molecular characterization of Epstein-Barr virus-positive plasmacytoma. Am J Surg Pathol. 2022;46(10):1364-1379.
47. Aguilera NS, Kapadia SB, Nalesnik MA, Swerdlow SH. Extramedullary plasmacytoma of the head and neck: use of paraffin sections to assess clonality with in situ hybridization, growth fraction, and the presence of Epstein-Barr virus. Mod Pathol. 1995;8(5):503-508.
48. Grande BM, Gerhard DS, Jiang A, et al. Genome-wide discovery of somatic coding and noncoding mutations in pediatric endemic and sporadic Burkitt lymphoma. Blood. 2019;133(12):1313-1324.
49. Yadav U, Kumar SK, Baughn LB, et al. Impact of cytogenetic abnormalities on the risk of disease progression in solitary bone plasmacytomas. Blood. 2023;142(22):1871-1878.

Tables

Table 1. Clinical characteristics of the EMP cohort.

Case	Sex	Age	Site	BM	Treatment	Follow-up[+]	PP	Additional information
1	m	18	Cervical LN	–	S+RT	29 mo – CR	–	History of classical Hodgkin lymphoma
2	f	70	Epipharynx	–*	RT	16 mo – CR	–	
3	f	71	Epipharynx	–*	S+RT	24 mo – DOC	+	Relapse; primary EMP 50 mo prior (larynx; S+RT); EMP in CR at death
4	f	46	Epipharynx	–*	S+RT	102 mo – CR	–	
5	f	47	Epipharynx	–	S+RT	64 mo – CR	–	
6	m	64	Paranasal sinuses	N/A	N/A	N/A	N/A	
7	m	64	Paranasal sinuses	–*	RT	143 mo – CR	–	Relapse 68 mo later (Paranasal sinuses; VRD followed by RD; RD discontinued due to toxicity)
8	m	55	Cervical LN	–*	S+RT	120 mo – CR	–	
9	f	55	Larynx	–	S+RT	176 mo – CR	–	
10	m	73	Epipharynx	–*	RT	141 mo – CR	–	Second relapse; primary EMP 15 mo prior (larynx; S+RT); first relapse 5 mo prior (epipharynx; S)
11	m	84	Oropharynx + cervical LN	–*	S+RT	7 mo – DOD	–	Progression to MM 6 mo later; no BM infiltration or paraprotein at EMP diagnosis
12	m	50	Oropharynx	–	S+RT	194 mo – CR	–	
13	f	59	Orbital soft tissue	–	RT	38 mo – AWR	–	Relapse 38 mo later (lacrimal gland; therapy not yet initiated at last FU)
14	m	74	Nasal cavity	–	RT	5 mo – CR	+	
15	m	69	Palatine tonsil + cervical LN	–	S+RT	8 mo – CR	–	History of primary myelofibrosis
16	m	93	Paranasal sinuses	N/A	W&W	3 mo – AWD	N/A	BM biopsy forgone (palliative setting); history of chronic lymphocytic leukemia
17	m	41	Nasal cavity	–*	S+RT	41 mo – CR	–	Relapse; primary EMP 48 mo prior (oropharynx; S)
18	m	74	Palatine tonsil + cervical LN	–*	RT	135 mo – DOC	+	EMP in CR at death
19	m	81	Epipharynx	–*	RT	N/A	–	
20	m	67	Oropharynx	–*	S	96 mo – SD	–	
21	m	62	Soft tissue of the thigh	–*	RT	31 mo – CR	+	
22	m	45	Cervical LN	–	N/A	7 mo – AWUS	N/A	
23	m	55	Lung + mediastinal LNs	–*	CT+ASCT	29 mo – CR	–	Treated with VRD followed by HDM/ASCT
24	m	59	Epipharynx	N/A	RT	12 mo – CR	–	BM biopsy forgone (no clinical evidence of MM)

A dash (–) indicates absence of the respective finding when used as a standalone entry. “BM” refers to the presence of bone marrow involvement as assessed by trephine biopsy. Cases marked with an asterisk (*) had available bone marrow flow cytometry data, none of which demonstrated clonal plasma cells. [+]Follow-up was calculated from the manifestation/lesion included in the cohort. AWD, alive with disease; AWR, alive with recurrence; AWUS, alive with unclear status; CR, complete remission; CT, chemotherapy; DOC, dead of other causes; DOD, dead of disease; mo, months; EMP, extramedullary plasmacytoma; HDM/ASCT, high-dose melphalan followed by autologous stem cell transplantation; N/A, information not available; PP, paraprotein; S, surgery; SD, stable disease; RD, lenalidomide, dexamethasone; RT, radiation therapy; VRD, bortezomib, lenalidomide, dexamethasone; W&W, watch and wait.

Table 2. Immunohistochemical findings.

Group	Case	CD56	Cyclin D1	MYC Score[$]	p53[*]	Ki67 (%)
EMP	1	–	–	1	WT	57.69
	2	+	–	0	WT	5.39
	3	–	–	0	WT	6.71
	4	–	–	1	WT	15.83
	5	–	–	1	WT	22.21
	6	–	–	1	WT	5.29
	7	–	–	0	WT	2.88
	8	–	–	1	WT	40.44
	9	–	–	0	WT	4.17
	10	–	–	1	WT	1.64
	11	–	+ (h)	1	WT	27.42
	12	+	–	0	WT	3.66
	13	+	–	0	WT	25.08
	14	–	–	2	WT	72.06
	15	–	–	1	WT	20.53
	16	–	–	2	WT	63.82
	17	–	–	1	WT	28.38
	18	–	–	0	WT	0.07
	19	–	–	1	WT	19.9
	20	+	–	0	WT	21.69
	21	+	–	0	WT	19.67
	22	+	–	0	WT	4.78
	23	+	+	0	+ (f)	7.42
	24	+	–	1	WT	61.66
EMD	25	+ (f)	–	N/A	N/A	N/A
	26	+	+ (h)	1	WT	41.05
	27	+	–	1	WT	56.9
	28	+ (f)	–	3	WT	76.83
	29	+	–	1	–	85.99
	30	–	+	0	WT	12.39
	31	–	–	3	+	39.97
	32	+	–	1	WT	42.22
	33	–	–	2	WT	71.65
	34	+	+	1	WT	35.69
	35	+	–	2	WT	36.66
	36	–	–	2	WT	77.46
	37	+	+ (h)	2	WT	32.99
	38	+	+ (h)	2	WT	23.55
	39	+	+ (h)	1	WT	7.88
	40	+	+ (h)	2	WT	28.13
	41	–	–	3	+	65.19
	42	–	–	1	WT	65.6
	43	+	+ (h)	2	WT	71.69
	44	–	–	0	WT	6.51
	45	–	+	0	WT	8.21
	46	+	–	3	WT	74.41
	47	+	–	N/A	N/A	50[#]
	48	+	–	1	–	61.4

EMD, extramedullary disease of multiple myeloma; EMP, extramedullary plasmacytoma; N/A, not available; WT, wild-type expression pattern; (f), focal positivity; (h), heterogeneous positivity. [$]MYC was scored as 0 (no expression), 1 (<30% positive cells), 2 (30–70% positive cells), and 3 (>70% positive cells). *Concerning p53, "(+)" indicates aberrant overexpression, whereas "(–)" designates complete loss of expression. [#]Manual evaluation.

Figure legends

Figure 1. Morphology and immunophenotype of EMP and EMD. (A) Hematoxylin and eosin (H&E) stain of an extramedullary plasmacytoma (EMP; case 15) infiltrating the palatine tonsil, with sheets of plasma cells beneath the squamous epithelium. The tumor cells demonstrate mature cytology with eccentric nuclei, ample cytoplasm, and inconspicuous nucleoli. Note the scattered binucleated forms (original magnifications ×100 and ×400). (B) H&E stain of extramedullary disease of multiple myeloma (EMD; case 33) involving the abdominal subcutaneous tissue. The tumor cells display immature cytology with an increased nucleus-to-cytoplasm ratio, prominent nucleoli, and frequent mitotic figures (×100 and ×400). (C) Immunohistochemical findings illustrating characteristic expression patterns. Upper left: Focal aberrant CD56 expression in the EMD of case 28 (top) and strong aberrant CD56 expression in the EMD of case 43 (bottom; ×200). Upper right: Heterogeneous aberrant Cyclin D1 expression in the EMD of case 43 (top), associated with hyperdiploidy (HD), and strong, homogeneous Cyclin D1 expression in the EMP of case 23 (bottom) due to an underlying *CCND1* rearrangement (*CCND1*-R) (×200). Bottom left: MYC expression in two EMD samples scored as 2 (top; case 43) and 3 (bottom; case 46), respectively (×400). Bottom right: Weak and heterogeneous p53 expression in the EMD of case 42 (top), corresponding to a *TP53* wild-type (WT) staining pattern, and strong p53 overexpression in the EMP of case 23 (bottom), consistent with a *TP53*-mutant (*TP53*mut) pattern (×400).

Figure 2. CNA frequency plots of EMP and EMD. The frequency of copy number alterations (CNA), i.e., gains and losses, is shown on the Y-axis, with the X-axis depicting chromosomes 1 through Y, from the p- to the q-arm. Alterations in extramedullary plasmacytoma (EMP) samples are shown in blue in the top panel (A), whereas those in extramedullary disease of multiple myeloma (EMD) samples are shown in red in the bottom panel (B).

Figure 3. Genetic landscape of EMP and EMD. Each column represents an individual case, and each row corresponds to a specific gene or cytogenetic alteration. The top bar plot indicates the number of mutated genes in each case: those with a variant allele frequency (VAF) <50% in light blue, VAF ≥50% in dark blue, and those with more than one mutation in red. The right bar plot displays the number of extramedullary plasmacytoma (EMP; blue) and extramedullary disease of multiple myeloma (EMD; red) cases harboring mutations in the respective gene. In underscored cases, chromosomal alterations reflect an integrated interpretation of fluorescence in situ hybridization and OncoScan analysis. "Chr17 gain + del(17p)" indicates a chromosomal gain accompanied by a relative *TP53* loss in cases 19, 20, and 46, whereas case 28 demonstrated a gain of chromosome 17 with an absolute *TP53* loss, i.e., with only one allele remaining.

Figure 1

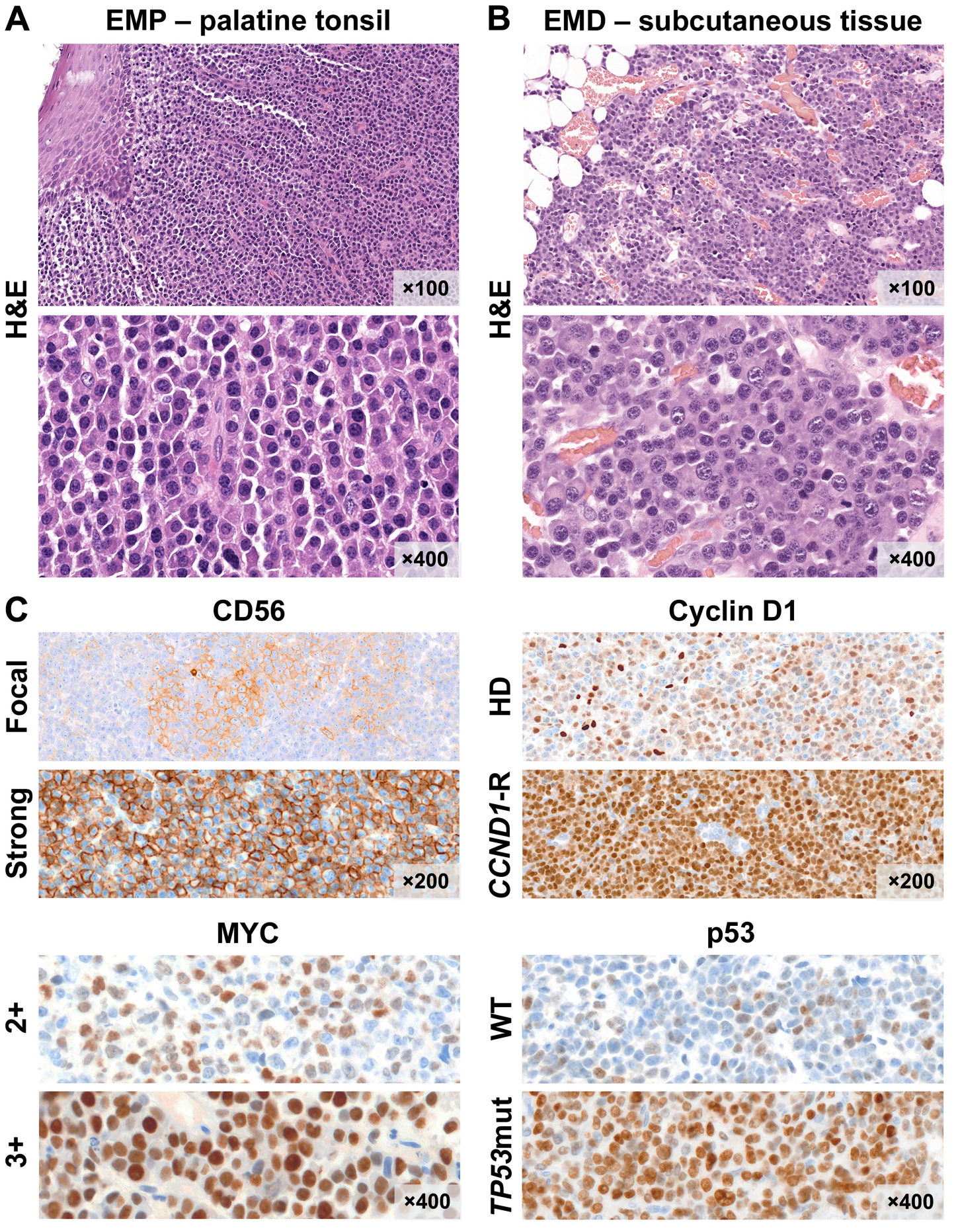
A
EMP – palatine tonsil
B
EMD – subcutaneous tissue
H&E
×100
×400
H&E
×100
×400
C
CD56
Cyclin D1
Focal
HD
Strong
CCND1-R
×200
×200
MYC
p53
2+
WT
3+
TP53mut
×400
×400

Figure 2

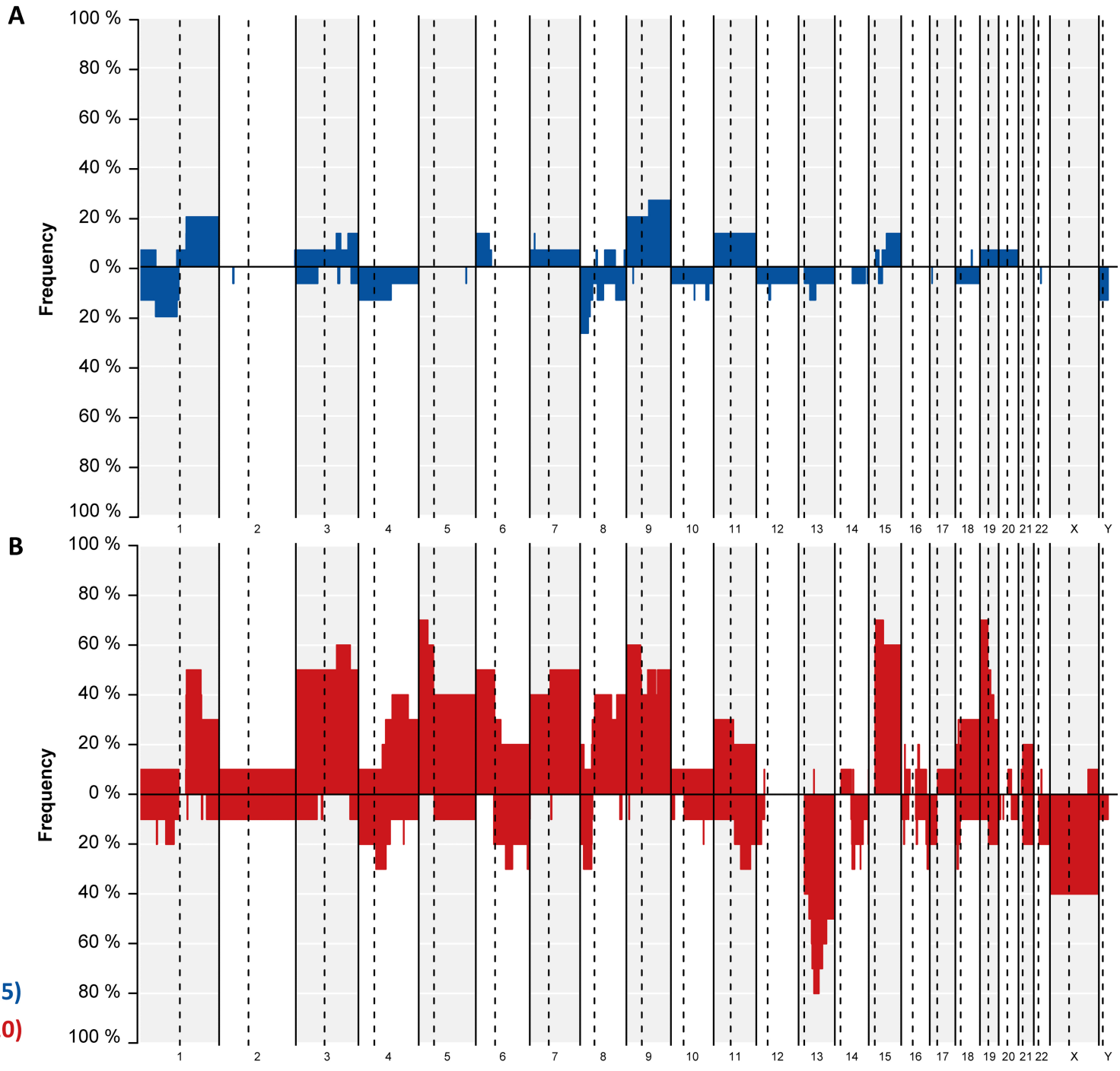
A
B
Frequency
100 %
80 %
60 %
40 %
20 %
0 %
1
2
3
4
5
6
7
8
9
10
11
12
13
14
15
16
17
18
19
20
21
22
X
Y
EMP (n=15)
EMD (n=10)

Figure 3

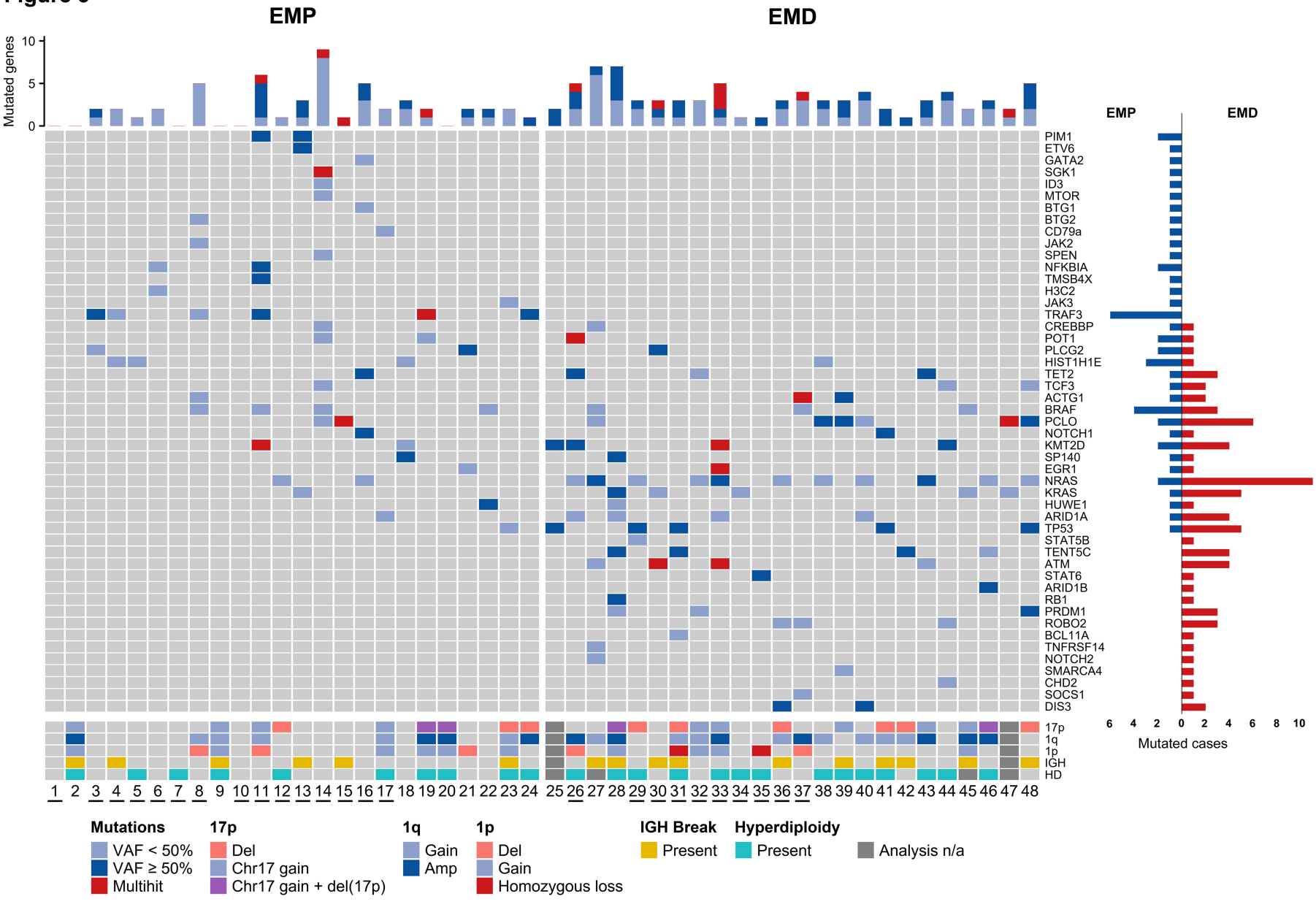
EMP
EMD
Mutated genes
10
5
0
PIM1
ETV6
GATA2
SGK1
ID3
MTOR
BTG1
BTG2
CD79a
JAK2
SPEN
NFKBIA
TMSB4X
H3C2
JAK3
TRAF3
CREBBP
POT1
PLCG2
HIST1H1E
TET2
TCF3
ACTG1
BRAF
PCLO
NOTCH1
KMT2D
SP140
EGR1
NRAS
KRAS
HUWE1
ARID1A
TP53
STAT5B
TENT5C
ATM
STAT6
ARID1B
RB1
PRDM1
ROBO2
BCL11A
TNFRSF14
NOTCH2
SMARCA4
CHD2
SOCS1
DIS3
EMP
EMD
6 4 2 0 2 4 6 8 10
Mutated cases
17p
1q
1p
IGH
HD
1 2 3 4 5 6 7 8 9 10 11 12 13 14 15 16 17 18 19 20 21 22 23 24 25 26 27 28 29 30 31 32 33 34 35 36 37 38 39 40 41 42 43 44 45 46 47 48
Mutations
VAF < 50%
VAF ≥ 50%
Multihit
17p
Del
Chr17 gain
Chr17 gain + del(17p)
1q
Gain
Amp
1p
Del
Gain
Homozygous loss
IGH Break
Present
Hyperdiploidy
Present
Analysis n/a

Supplemental Information

Vogelsberg et al.

Supplemental methods

Immunohistochemistry

Specimens were fixed in 4% buffered formalin and embedded in paraffin for histopathological analysis. Sections were stained with hematoxylin and eosin (H&E) and Giemsa. Immunostaining and EBV in situ hybridization were performed on an automated immunostainer (Ventana Benchmark XT, Ventana, Tucson, AZ, USA). All cases were stained for CD138 (ready-to-use [rtu], Roche, Basel, Switzerland), Cyclin D1 (rtu, Roche), CD56 (1:300, Menarini, Florence, Italy), c-MYC (rtu, Roche), immunoglobulin (IG) Kappa (1:25,000, Dako, Jena, Germany), IG Lambda (1:25,000, Dako), MIB1 (1:200, Dako), MUM1 (1:400, Dako), p53 (1:400, Novocastra, Newcastle upon Tyne, UK) and EBV-encoded RNA (rtu, Roche). In addition, a subset of cases was stained for IG heavy chains IgA (1:80,000, Roche), IgG (1:30,000, Dako), and IgM (1:10,000, Dako) as well as for CD3 (1:100, DCS, Hamburg, Germany) and CD20 (1:500, Dako).

Aberrant p53 staining was defined as either a uniform overexpression or a complete absence of p53 expression in the tumor cells. MYC expression was assessed quantitatively as described by Xiao et al., with each sample assigned a score of 0 (no expression), 1 (<30% positive cells), 2 (30–70% positive cells), or 3 (>70% positive cells).[1] Ki67 was assessed in one high-power field (diameter 0.55 mm) at the proliferation hotspot using automated image analysis with aetherAI software (version 105122, Taipei City, Taiwan), following digitization of the slides with the Pathology Scanner SG300 (Philips, Hamburg, Germany). Histological images were processed with Adobe Photoshop CS4 (version 11.0, Adobe Systems, San José, CA, USA).

Fluorescence *in situ* hybridization (FISH) and copy number (CN) analysis

FISH analysis was generally performed using the ZytoLight SPEC IGH Dual Color Break Apart Probe (ZytoVision, Bremerhaven, Germany), the ZytoLight SPEC CKS1B/CDKN2C Dual Color Probe (ZytoVision), the ZytoLight SPEC TP53/CEN 17 Dual Color Probe (ZytoVision), as well as the 5p15/9q22/15q22 Hyperdiploidy Amplification Probe (MetaSystems, Altlußheim, Germany) and was evaluated using the Axio Imager.M2 microscope equipped with the integrated ApoTome.2 system (Zeiss, Oberkochen, Germany). Extramedullary plasmacytoma (EMP) samples with an IGH translocation, as well as case 41, in which several spatially and temporally distinct manifestations were studied, were additionally analyzed using the Vysis LSI CCND1 Break Apart Rearrangement Probe (Abbott GmbH, Wiesbaden, Germany), the ZytoLight SPEC FGFR3/IGH Dual Color Dual Fusion Probe (ZytoVision), the ZytoLight SPEC MAF/IGH Dual Color Dual Fusion Probe (ZytoVision), and the ZytoLight SPEC MAFB/IGH Dual Color Dual Fusion Probe (ZytoVision). At least 50 nuclei were evaluated per sample and probe. Due to the use of FFPE tissue sections, which result in a higher background of aberrant fluorescence patterns, the threshold for numerical alterations was conservatively set at 40% of cells. In contrast, the threshold for IGH breaks was set at 10%, based on extensive prior validation of the IGH break-apart probe for routine diagnostics. A gain of both *CKS1B* (1q21.3–q22) and *CDKN2C* (1p32.3) was interpreted as a gain of chromosome 1 as a whole. Similarly, concurrent gains of *TP53* (17p13.1) and the centromeric reference probe were interpreted as polyploidy of chromosome 17. Amplification of 1q was defined by FISH as a gain with >3 fluorescence signals per nucleus.[2]

Concerning the CN analysis, CN alterations (CNA) with a minimum size of 100 kb and CN neutral losses of heterozygosity (CNN-LOH) larger than 5 Mb were considered informative, given that somatic CNA typically involve larger genomic regions than constitutional CN variations (CNV). To exclude larger constitutional CNV, we assessed the percentage of overlap with known CNV for alterations larger than 100 kb but smaller than 500 kb using the Database of Genomic Variants (DGV).[3] The human reference genome was GRCh37/hg19.

The cancer cell fraction (CCF) for each CNA was determined using ASCAT (v3.2.0). For each case (n=22) carrying CNA, the B-allele frequency (BAF) and logR values were derived from OncoScan data via Nexus Copy Number Software v9.0 (Bionano Genomics, San Diego, CA, USA). Tumor purity and ploidy estimates derived from ASCAT were used to adjust the predicted CCF, as previously reported and outlined below.[4,5] Although these formulas were defined for near-diploid tumors, they were adapted accordingly for polyploid cases.

$$\mathbf{CCF_{CN\ LOSS}} = \frac{(-2 * \mathrm{BAF} + 1)}{(1 - \mathrm{BAF})} \longrightarrow \boxed{\mathbf{Corrected\ CCF_{CN\ LOSS}} = \frac{\mathrm{CCF_{CN\ LOSS}}}{\mathrm{Purity}}}$$

$$\mathbf{CCF_{CN\ GAIN}} = \frac{(2 * \mathrm{BAF} + 1)}{(\mathrm{major} - 1) - \big((\mathrm{major} - 1) * \mathrm{BAF}\big) - ((\mathrm{minor} - 1) * \mathrm{BAF}))} \longrightarrow \boxed{\mathbf{Corrected\ CCF_{CN\ GAIN}} = \frac{\mathrm{CCF_{CN\ GAIN}}}{\mathrm{Purity}}}$$

$$\mathbf{CCF_{CN\ LOH}} = \frac{(2 * \mathrm{B} + 1)}{(1 - \mathrm{BAF})} \longrightarrow \boxed{\mathbf{Corrected\ CCF_{CNN-LOH}} = \frac{\mathrm{CCF_{CNN-LOH}}}{\mathrm{Purity}}}$$

For two samples (cases 11 and 33) that ASCAT predicted as polyploid, manual normalization was performed, assigning the diploid region at the level of chromosomes 6/13 and 12, respectively.[6] Hyperdiploidy was defined as trisomy of three or more of the odd-numbered chromosomes 3, 5, 7, 9, 11, 15, 19, and/or 21.[7] For the genomic complexity analysis, hyperdiploid chromosomes were counted as separate chromosomal aberrations. For samples analyzed by FISH only, hyperdiploidy was defined as gains of any two of the chromosome 5, 9, or 15 probes.[8,9] The final CN profile reflects the integration of FISH and CN analyses. In cases with discrepancies, the FISH results served as ground truth, owing to their single-cell resolution and higher reliability in degraded samples.[10,11]

Targeted next-generation sequencing analysis

Library preparation and sequencing

Amplicon library preparation and semiconductor sequencing were performed according to the instructions of the manufacturer using the Ion AmpliSeq Library Kit 2.0/Plus, the Ion Library TaqMan Quantitation Kit, the Ion 510 & Ion 520 & Ion 530 Kit - Chef/the Ion 540 Kit - Chef, and the Ion 530/540 Chip Kit (Thermo Fisher Scientific, Waltham, MA, USA). In brief, for each primer pool, 10 ng of DNA were combined with the AmpliSeq HiFi Mix (Thermo Fisher Scientific) and the respective primer sets to amplify the target regions. Subsequently, the primer end sequences were partially digested using FuPa reagent (Thermo Fisher Scientific), followed by the ligation of barcoded sequencing adapters (Ion Xpress Barcode Adapters; Thermo Fisher Scientific). The final libraries were purified using AMPure XP magnetic beads (Beckman Coulter, Brea, CA, USA), quantified using qPCR on the QuantStudio 5 Dx Real-Time PCR System (Thermo Fisher Scientific) and then pooled. Processing of the library pool, including attachment of DNA fragments to Ion Sphere Particles (ISPs), clonal amplification, and enrichment of template-positive ISPs, was performed with the Ion Chef platform (Thermo Fisher Scientific). Sequencing was performed on the Ion GeneStudio S5 Prime using the Ion 530/540 Chip Kit (Thermo Fisher Scientific).

Alignment, variant calling, and filtering

Raw data analysis was performed using the Ion Torrent Software Suite (version 5.16.1, Thermo Fisher Scientific). The reads were aligned to the human reference genome GRCh37/hg19. Bioinformatic analysis was conducted using the Ion Reporter Software (version 5.18.2.0, Thermo Fisher Scientific). Intronic and synonymous variants, as well as known polymorphisms, identified via public databases and online tools such as dbSNP, gnomAD, and VarSome, were excluded.[12,13] Panel-specific and fixation-related artifacts were excluded by visualizing all variants using the Integrative Genomics Viewer (Broad Institute, Cambridge, MA, USA). Furthermore, in cases with limited DNA integrity, the detection threshold, generally set at an allele frequency of 5%, was adjusted individually to account for the increased number of sequencing artifacts.

Supplemental results

Concordance of FISH and OncoScan

FISH and OncoScan were concordant for hyperdiploidy and chromosome 1 and 17 alterations in 86% of calls, including both aberrant and wild-type findings. Differences could largely be attributed to methodological characteristics of the respective platforms. Very focal CN losses of 1p32.3 and 17p13.1 detected by OncoScan were not detected by FISH, whereas FISH showed higher sensitivity in samples with tumor cell purity <50% (Supplemental Table S4).

Detailed CNA profiles of EMP and EMD

CNA in EMP consisted of 35 CN losses, 1 homozygous deletion, 28 gains, 1 amplification, and 7 CNN-LOH events, whereas the extramedullary disease of multiple myeloma (EMD) samples harbored 84 losses, 7 homozygous deletions, 84 gains, 18 amplifications, and 30 CNN-LOH events (Supplemental Figures S3 and S4; Supplemental Tables S4 and S5). The most recurrent CNA in EMD were losses of 13q14.2–q21.31 (8/10 samples), followed by gains of 5p15.33–p14.1, 15q11.2–q21.1, and 19p (each in 7/10), gains of 3q22.1–q26.31 and 9p (6/10) and gains of 1q21.1–q31.2, 6p, 7q, and 9q (5/10). The most frequent CNN-LOH regions in EMD were located at 20p12.1–p11.21 and 9q22.2–q22.33 (each in 3/10).

CNA comparison with multiple myeloma (MM)

The comparison of the EMD samples with previously published CN data from two MM cohorts (https://www.ncbi.nlm.nih.gov/geo/query/acc.cgi?acc=GSE70399; https://www.ncbi.nlm.nih.gov/geo/query/acc.cgi?acc=GSE31339) revealed higher genomic complexity in EMD, with significantly more CNN-LOH events (mean 3.0 vs. 1.3 per case; $p < 0.05$)

and a trend toward a higher number of CNA (mean 19.3 vs. 12.9; $p = 0.065$).[14,15] No individual CNA region was significantly enriched in either group (Supplemental Figure S6).

Supplemental references

1. Xiao R, Cerny J, Devitt K, et al. MYC protein expression is detected in plasma cell myeloma but not in monoclonal gammopathy of undetermined significance (MGUS). Am J Surg Pathol. 2014;38(6):776–783.
2. Clarke SE, Fuller KA, Erber WN. Chromosomal defects in multiple myeloma. Blood Rev. 2024;64(101168.
3. MacDonald JR, Ziman R, Yuen RK, Feuk L, Scherer SW. The Database of Genomic Variants: a curated collection of structural variation in the human genome. Nucleic Acids Res. 2014;42(Database issue):D986–992.
4. Nadeu F, Clot G, Delgado J, et al. Clinical impact of the subclonal architecture and mutational complexity in chronic lymphocytic leukemia. Leukemia. 2018;32(3):645–653.
5. Ramis-Zaldivar JE, Gonzalez-Farre B, Nicolae A, et al. MAPK and JAK-STAT pathways dysregulation in plasmablastic lymphoma. Haematologica. 2021;106(10):2682–2693.
6. Ross EM, Haase K, Van Loo P, Markowetz F. Allele-specific multi-sample copy number segmentation in ASCAT. Bioinformatics. 2021;37(13):1909–1911.
7. Kuehl WM, Bergsagel PL. Molecular pathogenesis of multiple myeloma and its premalignant precursor. The Journal of clinical investigation. 2012;122(10):3456–3463.
8. Wuilleme S, Robillard N, Lodé L, et al. Ploidy, as detected by fluorescence in situ hybridization, defines different subgroups in multiple myeloma. Leukemia. 2005;19(2):275–278.
9. Walker BA, Leone PE, Chiecchio L, et al. A compendium of myeloma-associated chromosomal copy number abnormalities and their prognostic value. Blood. 2010;116(15):e56–65.
10. Leeksma AC, Baliakas P, Moysiadis T, et al. Genomic arrays identify high-risk chronic lymphocytic leukemia with genomic complexity: a multi-center study. Haematologica. 2021;106(1):87–97.
11. Horn H, Bausinger J, Staiger AM, et al. Numerical and structural genomic aberrations are reliably detectable in tissue microarrays of formalin-fixed paraffin-embedded tumor samples by fluorescence in-situ hybridization. PLoS One. 2014;9(4):e95047.
12. Karczewski KJ, Francioli LC, Tiao G, et al. The mutational constraint spectrum quantified from variation in 141,456 humans. Nature. 2020;581(7809):434–443.
13. Kopanos C, Tsiolkas V, Kouris A, et al. VarSome: the human genomic variant search engine. Bioinformatics. 2019;35(11):1978–1980.
14. López-Corral L, Sarasquete ME, Beà S, et al. SNP-based mapping arrays reveal high genomic complexity in monoclonal gammopathies, from MGUS to myeloma status. Leukemia. 2012;26(12):2521–2529.
15. Paiva B, Corchete LA, Vidriales MB, et al. Phenotypic and genomic analysis of multiple myeloma minimal residual disease tumor cells: a new model to understand chemoresistance. Blood. 2016;127(15):1896–1906.

Supplemental tables

The following tables are provided in a separate file:

Supplemental Table S1. First AmpliSeq custom panel used for next-generation sequencing analysis.

Supplemental Table S2. Second AmpliSeq custom panel used for next-generation sequencing analysis.

Supplemental Table S3. Clinical characteristics of the EMD cohort.

Supplemental Table S4. Overview of copy number alterations and copy number neutral losses of heterozygosity.

Supplemental Table S5. Summary of copy number alterations and copy number neutral losses of heterozygosity.

Supplemental Table S6. Detailed results of the mutational analysis.

Supplemental figures

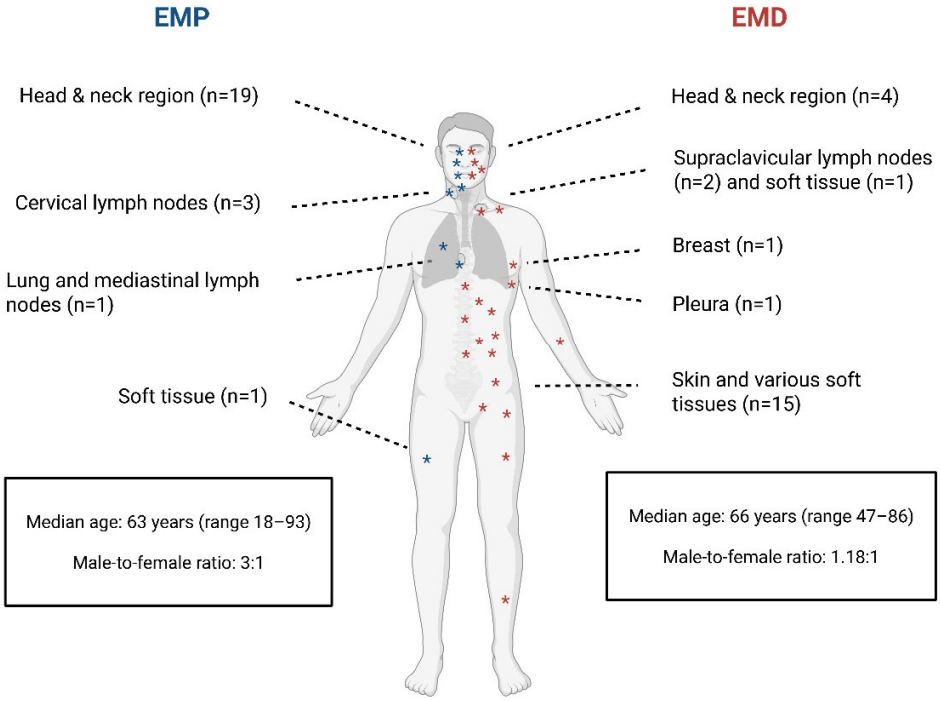

Supplemental Figure S1. Anatomical distribution and patient characteristics. Schematic body map with asterisks indicating sites of manifestation. Extramedullary plasmacytoma (EMP) is shown on the left and extramedullary disease of multiple myeloma (EMD) on the right. In EMP, cervical lymph node involvement is only depicted when it represented the primary site of manifestation. Created in BioRender. Vogelsberg, A. (2026) https://BioRender.com/bx2fgh8.

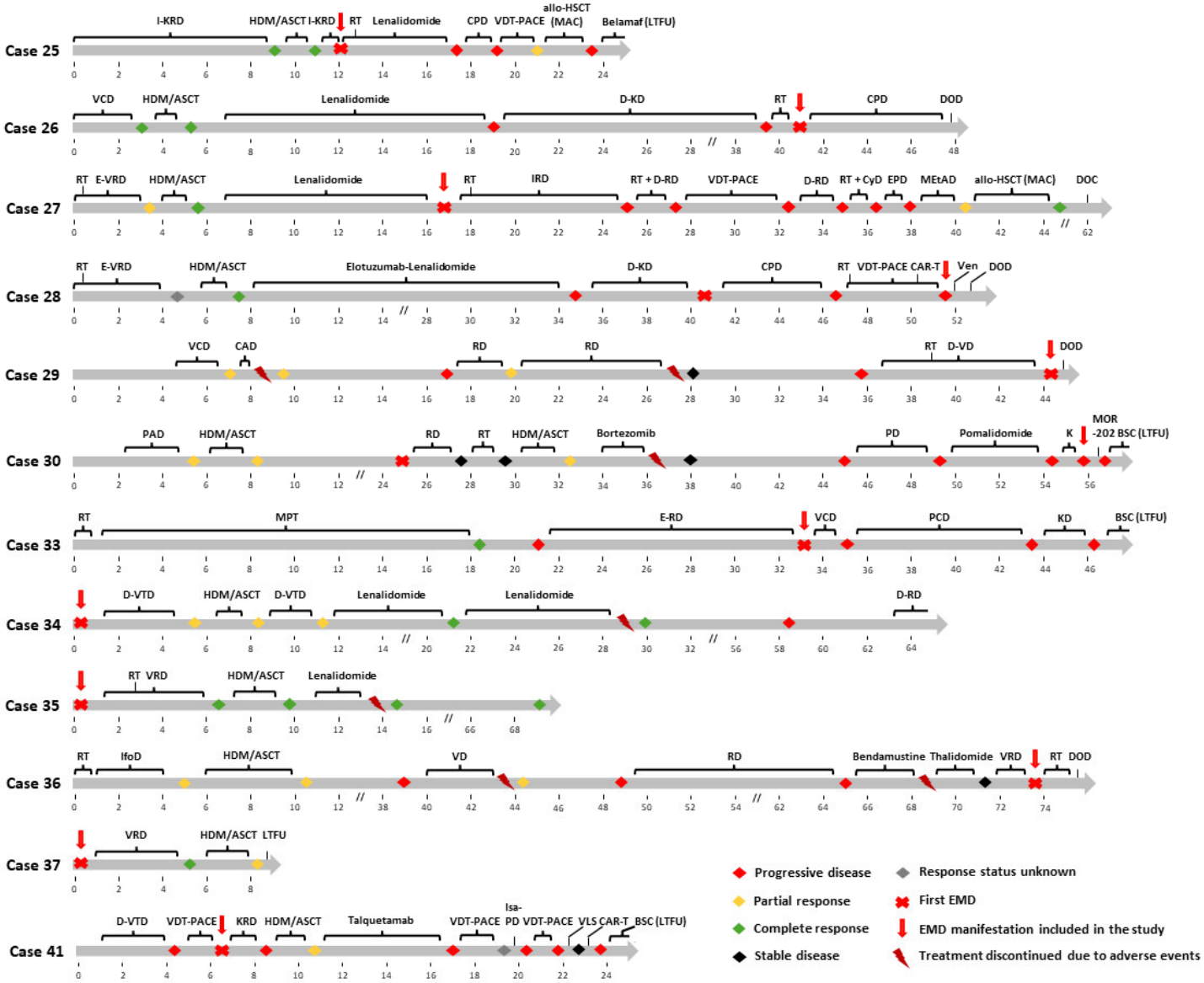
Case 25
I-KRD
HDM/ASCT
I-KRD
RT
Lenalidomide
CPD
VDT-PACE
allo-HSCT (MAC)
Belamaf (LTFU)
Case 26
VCD
HDM/ASCT
Lenalidomide
D-KD
RT
CPD
DOD
Case 27
RT
E-VRD
HDM/ASCT
Lenalidomide
RT
IRD
RT + D-RD
VDT-PACE
D-RD
RT + CyD
EPD
MEtAD
allo-HSCT (MAC)
DOC
Case 28
RT
E-VRD
HDM/ASCT
Elotuzumab-Lenalidomide
D-KD
CPD
RT
VDT-PACE
CAR-T
Ven
DOD
Case 29
VCD
CAD
RD
RD
RT
D-VD
DOD
Case 30
PAD
HDM/ASCT
RD
RT
HDM/ASCT
Bortezomib
PD
Pomalidomide
K
MOR -202
BSC (LTFU)
Case 33
RT
MPT
E-RD
VCD
PCD
KD
BSC (LTFU)
Case 34
D-VTD
HDM/ASCT
D-VTD
Lenalidomide
Lenalidomide
D-RD
Case 35
RT
VRD
HDM/ASCT
Lenalidomide
Case 36
RT
IfoD
HDM/ASCT
VD
RD
Bendamustine
Thalidomide
VRD
RT
DOD
Case 37
VRD
HDM/ASCT
LTFU
Case 41
D-VTD
VDT-PACE
KRD
HDM/ASCT
Talquetamab
VDT-PACE
Isa-PD
VDT-PACE
VLS
CAR-T
BSC (LTFU)
Progressive disease
Partial response
Complete response
Stable disease
Response status unknown
First EMD
EMD manifestation included in the study
Treatment discontinued due to adverse events

Supplemental Figure S2. Swimmer plot of clinical course and treatments in EMD patients. Only EMD patients with sufficient longitudinal clinical data were included. General abbreviations: LTFU, lost to follow-up; EMD, extramedullary disease; DOD, died of disease; DOC, died of other causes. Abbreviations of treatment regimens and agents (regimen abbreviations indicate the presence of agents and do not reflect dose or schedule)**:** allo-HSCT (MAC), allogeneic hematopoietic stem cell transplantation with myeloablative conditioning; Belamaf, belantamab mafodotin; BSC, best supportive care; CAD, cyclophosphamide, doxorubicin, dexamethasone; CAR-T, B-cell maturation antigen–directed chimeric antigen receptor T-cell therapy; CPD, cyclophosphamide, pomalidomide, dexamethasone; CyD, cyclophosphamide and dexamethasone; D-KD, daratumumab, carfilzomib, dexamethasone; D-RD, daratumumab, lenalidomide, dexamethasone; D-VD, daratumumab, bortezomib, dexamethasone; D-VTD, daratumumab, bortezomib, thalidomide, dexamethasone; EPD, elotuzumab, pomalidomide, dexamethasone; E-RD, elotuzumab, lenalidomide, dexamethasone; E-VRD, elotuzumab, bortezomib, lenalidomide, dexamethasone; HDM/ASCT, high-dose melphalan followed by autologous stem cell transplantation; I-KRD, isatuximab, carfilzomib, lenalidomide, dexamethasone; IfoD, ifosfamide and dexamethasone; IRD, ixazomib, lenalidomide, dexamethasone; Isa-PD, isatuximab, pomalidomide, dexamethasone; K, carfilzomib; KD, carfilzomib and dexamethasone; KRD, carfilzomib, lenalidomide, dexamethasone; MEtAD, methotrexate, etoposide, cytarabine, dexamethasone; MOR202, anti-CD38 monoclonal antibody; MPT, melphalan, prednisone, thalidomide; PAD, bortezomib, doxorubicin, dexamethasone; PCD, pomalidomide, cyclophosphamide, dexamethasone; PD, pomalidomide and dexamethasone; RD, lenalidomide and dexamethasone; RT, radiotherapy; VCD, bortezomib, cyclophosphamide, dexamethasone; VD, bortezomib and dexamethasone; VDT-PACE, bortezomib, dexamethasone, thalidomide, cisplatin, doxorubicin, cyclophosphamide, etoposide; Ven, venetoclax; VLS, venetoclax, lenalidomide, selinexor; VRD, bortezomib, lenalidomide, dexamethasone; VTD, bortezomib, thalidomide, dexamethasone.

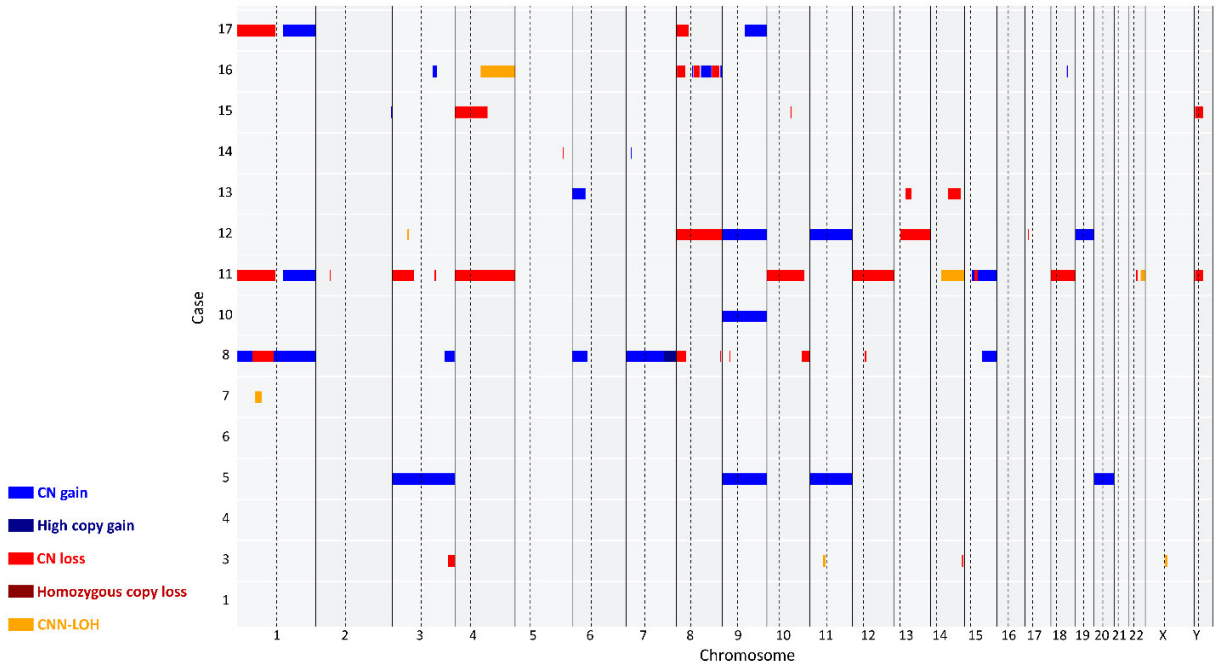

Supplemental Figure S3. Individual CN and CNN-LOH profiles of the EMP cases. Each row corresponds to a single case of extramedullary plasmacytoma (EMP). The presence of each alteration, i.e., copy number (CN) gains and losses, as well as copy number neutral loss of heterozygosity (CNN-LOH), is depicted along the X-axis across chromosomes 1 through Y, from the p- to the q-arm**.**

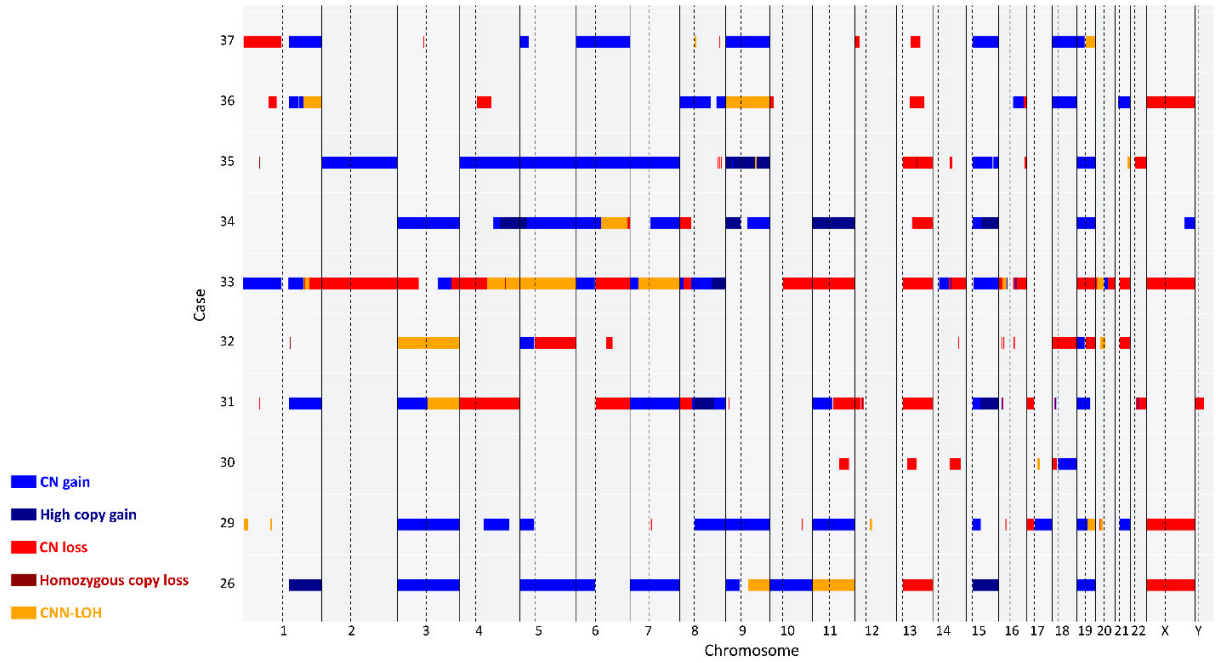

Supplemental Figure S4. Individual CN and CNN-LOH profiles of the EMD cases. Each row corresponds to a single case of extramedullary disease of multiple myeloma (EMD). The presence of each alteration, i.e., copy number (CN) gains and losses, as well as copy number neutral loss of heterozygosity (CNN-LOH), is depicted along the X-axis across chromosomes 1 through Y, from the p- to the q-arm.

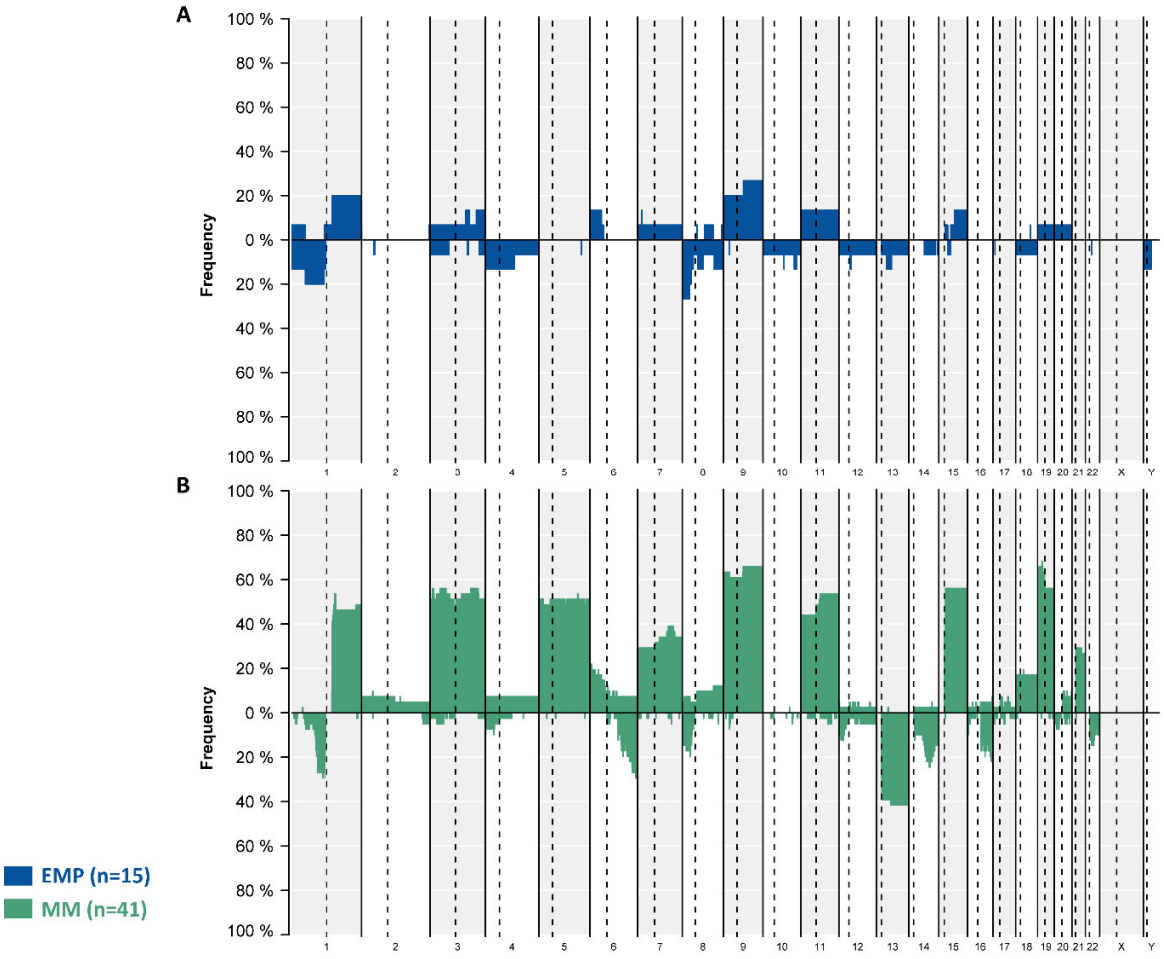

Supplemental Figure S5. CNA frequency plots of the EMP cohort and two previously published MM series. The frequency of copy number alterations (CNA), i.e., gains and losses, is shown on the Y-axis, with the X-axis depicting chromosomes 1 through Y, from the p- to the q-arm. Alterations of the extramedullary plasmacytoma (EMP) samples are shown in blue in the top panel (A), whereas those of two previously published series of multiple myeloma (MM) are shown in green in the bottom panel (B).

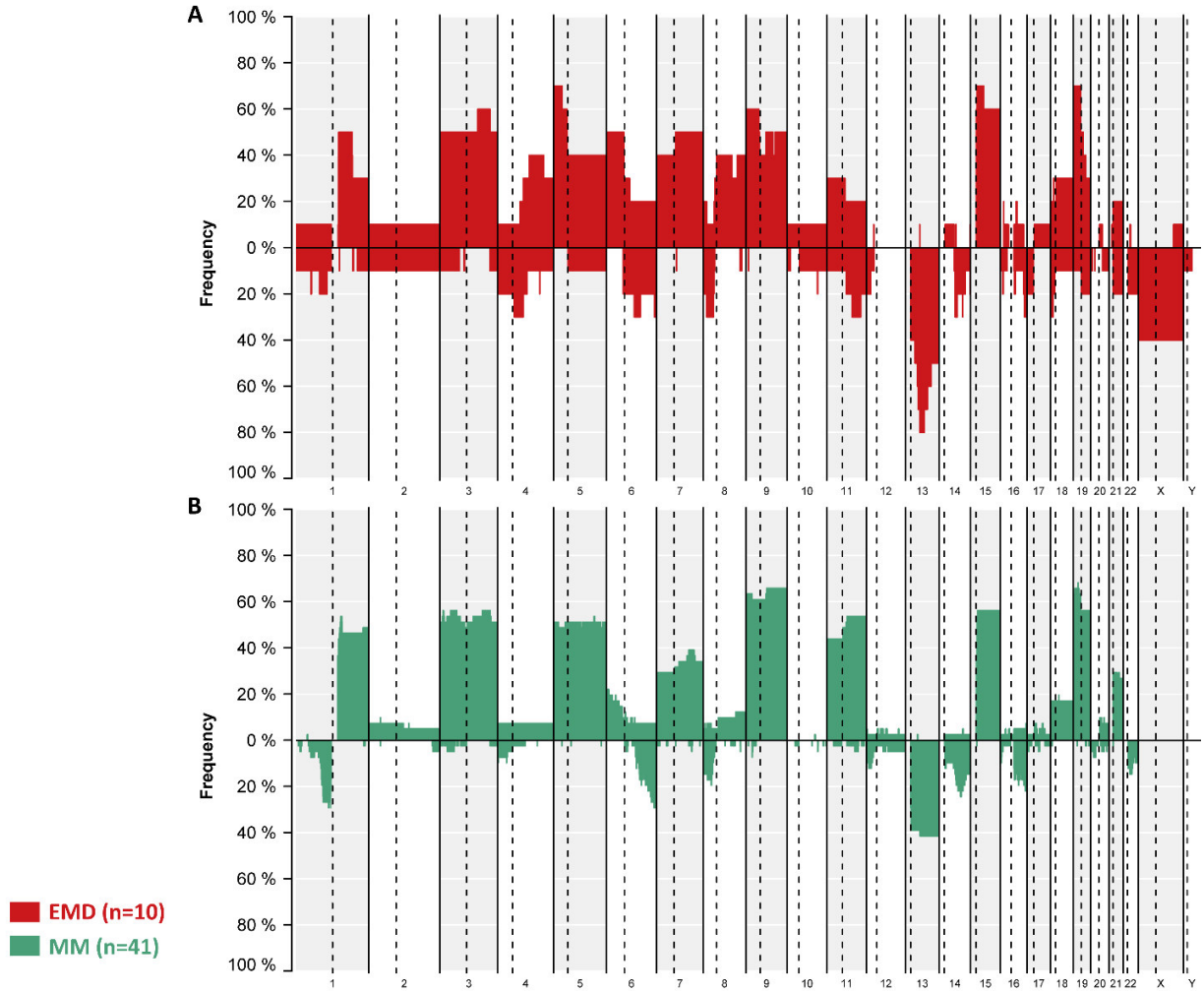

Supplemental Figure S6. CNA frequency plots of the EMD cohort and two previously published MM series. The frequency of copy number alterations (CNA), i.e., gains and losses, is shown on the Y-axis, with the X-axis depicting chromosomes 1 through Y, from the p- to the q-arm. Alterations of the extramedullary disease of multiple myeloma (EMD) samples are shown in red in the top panel (A), whereas those of two previously published series of multiple myeloma (MM) are shown in green in the bottom panel (B).

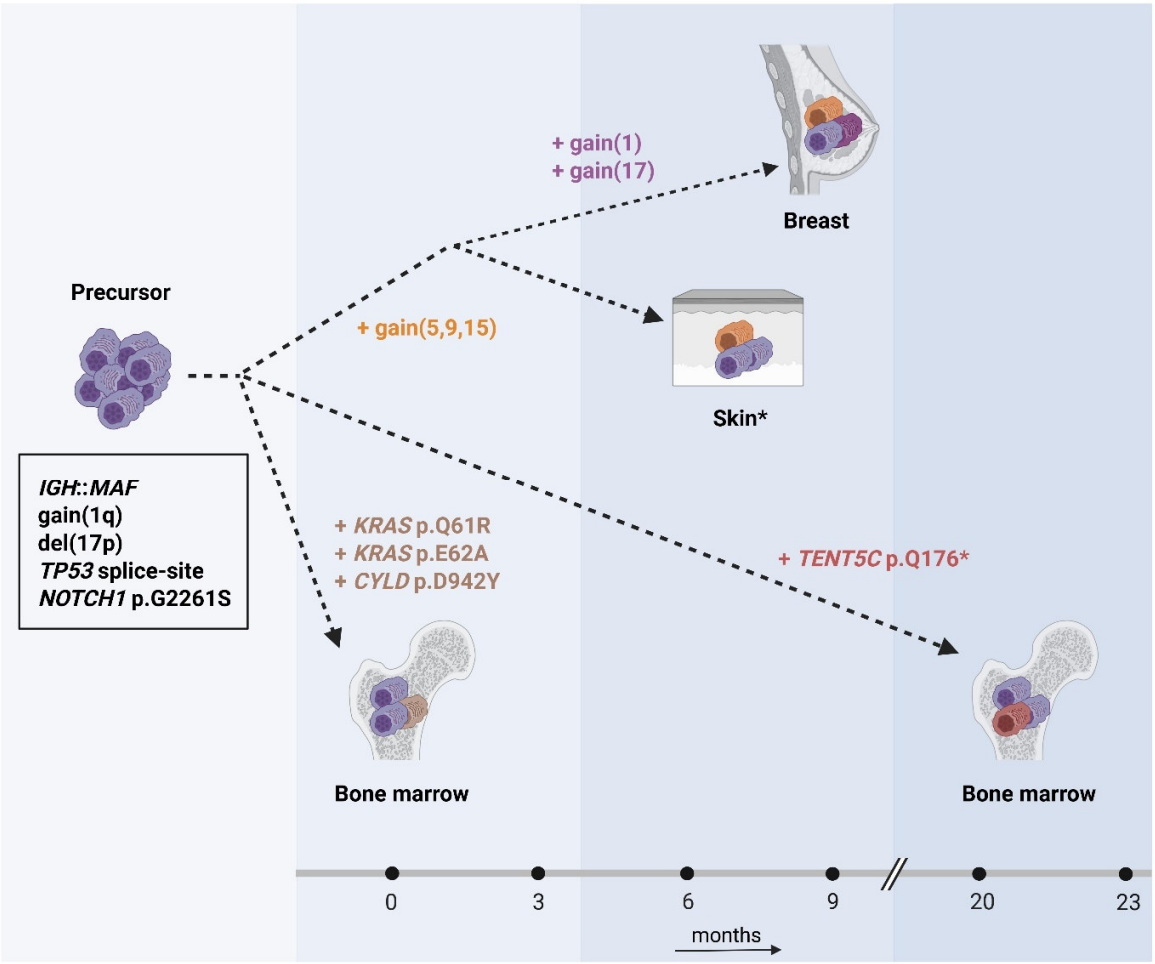

Supplemental Figure S7. Illustration of intraclonal heterogeneity in MM. Reconstruction of the clonal evolution of different multiple myeloma (MM) manifestations occurring at different time points and anatomical sites in patient 41. The asterisk (*) marks the sample included in the comparative analyses with extramedullary plasmacytoma. Chromosomal alterations are based on fluorescence in situ hybridization (FISH). All MM manifestations shared an *IGH*::*MAF* fusion, gain(1q), del(17p), as well as mutations in *TP53* and *NOTCH1*, indicating that these alterations were acquired in a common precursor clone, with the fusion presumably representing the initiating event. Both extramedullary manifestations additionally demonstrated hyperdiploidy (gains of chromosomes 5, 9, and 15) and therefore most likely originated from the same subclone, with the breast manifestation harboring further gains of chromosomes 1 and 17. In contrast, the bone marrow samples harbored private mutations in *KRAS* and *CYLD*, as well as *TENT5C*, respectively, but did not show additional gains of the chromosomes analyzed by FISH. Created in BioRender. Vogelsberg, A. (2026) https://BioRender.com/v39b5af.

Click here to access/download

Supplementary Excel Table

Supp_Tables.xlsx